Transient rivers characterize evolving crustal-scale flexure in the Corinth Rift

David Fernández-Blanco[1], Gino de Gelder[1], Sean Gallen[2], Robin Lacassin[1] and Rolando Armijo[1]

[1] Institut de Physique du Globe de Paris, Sorbonne Paris Cité, Univ Paris Diderot, UMR 7154 CNRS, F-75005 Paris, France

[2] Geological Institute, Swiss Federal Institute of Technology (ETH), 8092 Zürich, Switzerland

Abstract

Crustal elastic flexure on the flanks of rift-forming faults is a key feature to characterize continental rifting processes that can be resolved by means of transient river drainages on rift footwalls. Here we show that the elastic flexure dynamics of the uplifting southern shoulder of the rapidly-extending, asymmetric Corinth Rift (Greece) are recorded in 3D by its fluvial network. We explore the evolution of the mechanical flexure of the lithosphere at rift full length by means of DEM-based river profile analysis of a series of footwall catchments that drain roughly orthogonal to the rift active fault system. We show that elastic footwall flexure describes the first-order geometry of river longitudinal profiles. Flexure amplitude is maximal in the centre of the rift, where drainage reversal of two catchments suggests very fast slip rates on the active fault system, and decays *(i)* gently to the west, where transient river profiles exhibit a morphology consistent with relatively lower rates of flexural uplift and there exists evidence for active drainage reorganization, and *(ii)* sharply to the east, where river profiles are near equilibrium with the modern displacement field. These observations are consistent with landscape responding to growth of a new master fault as a function of slip rate increases and/or onset time. The occurrence of drainage reversal by footwall flexure in the rift centre suggests an extremely rapid footwall flexural uplift due to a sharp increase in master fault slip rate. Lateral changes in river morphology along the rift margin are consistent with either smaller rates of footwall flexural uplift or younger onset of faulting along strike away from the center of the master fault. Further, the extent of flexure, over the full length of the Corinth Rift (~100 km), requires a steep fault growing in a strong crust. These observations are at odds with Corinth Rift growth models of protracted extension and parallel basinwards-migrating faults linked or not at depth with a shallow detachment. To the contrary, our results support the hypothesis of rift growth by lateral along-strike addition of fault segments triggered by a recent shift in plate boundary conditions <1 Ma, an evolution compatible with the southwestwards process zone tip propagation of the North Anatolian Fault.

Keywords: Corinth Rift, continental rift, elastic flexure, footwall uplift, footwall rivers, river profile analysis

Highlights

Footwall river profiles in Corinth Rift main shoulder report crustal elastic flexure

Footwall elastic flexure relates with new master fault growing laterally along strike

Flexure in high-angle crustal master fault refutes rift models of continuous growth

Abrupt change in master fault uplift rate in rift centre forced large river reversals

Flexure along-strike asymmetry reflects fault varying uplift rates and/or onset times

Graphical abstract

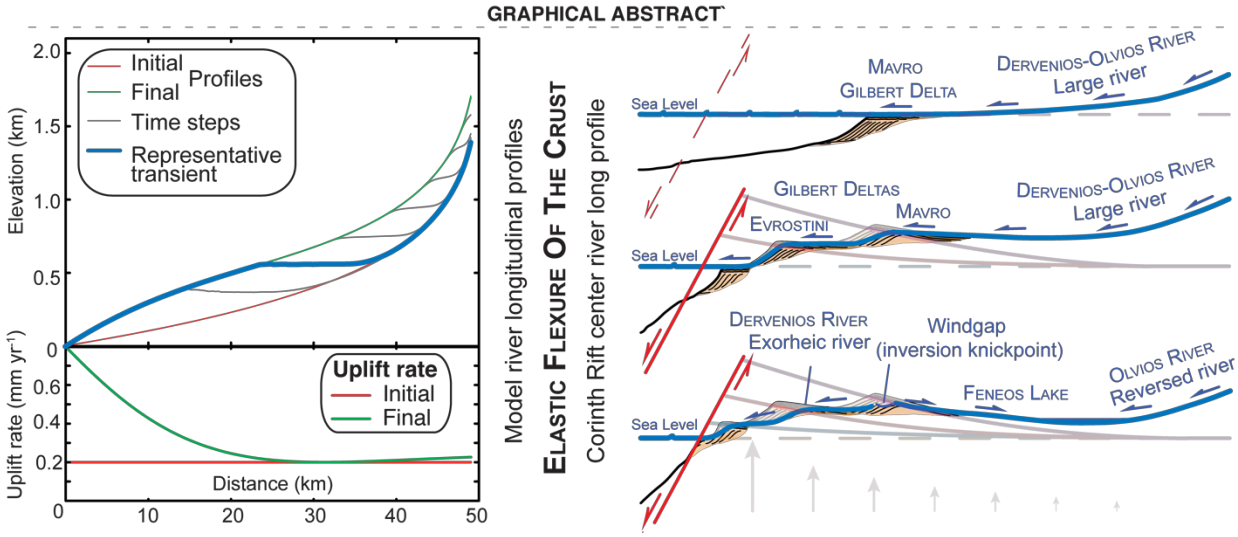

1. Introduction

Continental regions undergoing extension such as intracontinental rifts often show localized flexural uplift, i.e. kilometers of uplift expressed for several tens of kilometers along strike and decaying exponentially within few tens of kilometers across strike (e.g., King et al., 1988; Weissel and Karner, 1989; King and Ellis, 1990). In these regions, high topography supported by flexural isostasy can be explained by planar high-angle normal faults in a thick plate (e.g., Buck, 1991). Contrarily, low-angle faults growing in a thin lithosphere develop little to none elastic flexure (e.g., Forsyth, 1992; Buck, 1993). It follows that characterizing elastic flexure associated with rift flank uplift is essential to discriminate possible fault geometries at depth (e.g., Resor and Pollard, 2012), and therefore to differentiate among mechanical models of rift extension.

The amagmatic continental rift of Corinth is the most seismically active and fastest extending continental region in Europe, with extension rates of ~1-1.5 $cm \times yr^{-1}$ (e.g., Avallone et al., 2004; Bernard et al., 2006) due to slip on steep upper-crust normal faults whose geometry at depth is disputed (e.g., Bell et al., 2017; Rigo et al., 1996). The modern Corinth Rift is young (between <5 and <1 Ma) and markedly asymmetric in relation to its north-dipping master fault system, composed of several en-échelon normal fault segments with a cumulative length of ~130 km (Fig. 1) (e.g., Armijo et al., 1996; Ford et al., 2016). This fault system has propelled the growth of >5 km of structural relief since <1 Ma in the southern shoulder of the rift (e.g., Armijo et al., 1996; Nixon et al., 2016). Several rift growth models are proposed to explain this remarkable Late Quaternary faulting. Sequential rift narrowing and successive basinward fault migration is a well-accepted mechanism proposed originally by Goldsworthy and Jackson (2001). Rigo et al. (1996) and Sorel (2000) suggest that the steep faults observed at surface sole out into a north-dipping shallow detachment, a mechanism that is often framed in the context of continued Aegean extension (e.g., Jolivet et al., 2010). Models without an intervening low-angle detachment show that total rift extension estimated by aggregation of fault heaves under the assumption of planar geometry agrees with the observed crustal thinning (e.g., McNeill et al, 2005; Bell et al., 2011). “Tilted block” models

(with or without a detachment) dismiss the elastic flexure of the rift main footwall and the changes in plate boundary conditions imposed by the propagation of the North Anatolian Fault into the Aegean (Armijo et al., 1996).

In the eastern sector of the Corinth Rift main shoulder, between Xylokastro and Corinth (Fig. 1), localized deformation marked by a flight of uplifted marine terraces is consistent with upward footwall elastic flexure (Armijo et al., 1996; de Gelder et al., 2017). The state and extent of such flexure remains unexplored along strike of the rift master fault system. Here, we explore footwall flexure along the full Corinth Rift southern shoulder analyzing footwall catchments that drain orthogonally towards the hanging wall, as well as proximal, recently-reversed endorheic river basins. We use 20m-resolution DEM-based analysis of river longitudinal profiles and profiles transformed through the integral quantity χ (χ-profiles) to characterize elastic flexure of the main fault system along the rift strike. Since footwall flexure depends on fault geometry at depth and the strength of the crust, we do not only gain understanding on crustal flexure effects on relief evolution in the Corinth Rift southern margin but also on its mechanical evolution.

Fig. 1. Tectonomorphologic and active tectonics map of the Gulf of Corinth, with focus set on the river networks and main fault systems studied in this contribution. Inlet at the centre-top provides a synthetic view of the main geologic units. Basement units are simplified from Taylor et al., 2011, and fill units are slightly from Armijo et al., 2006. Inlet at the right-top is the index map of the main river networks draining the southern shoulder of the Corinth Rift, from east to west: (1) Xerias; (2) Raizanis; (3) Zapantis; (4) Asopos; (5) Trikalitikos; (6) Fonissa; (7) Skoupeiko; (8) Dervenios; (9) Krios; (10) Krathis; (11) Ladopotamos; (12) Vouraikos; (13) Kerinitis; (14) Selinous; (15) Meganitis; and (16) Finikas. The internally drained basins and their rivers are from east to west: (A) Skotini and the Souteni River; (B) Stymfalia and the Safenetos River; and (C) Feneos and the Olvios River. Faults segments from the master mentioned in this contribution are abbreviated (from east to west) as: Xylokastro Fault, Offshore (Xy Off) and Onshore (Xy On); Lykoporia (Ly); Derveni (De); Eliki Fault, West (W Ek) and East (E Ek). Location of figures 4-B and 8 is shown.

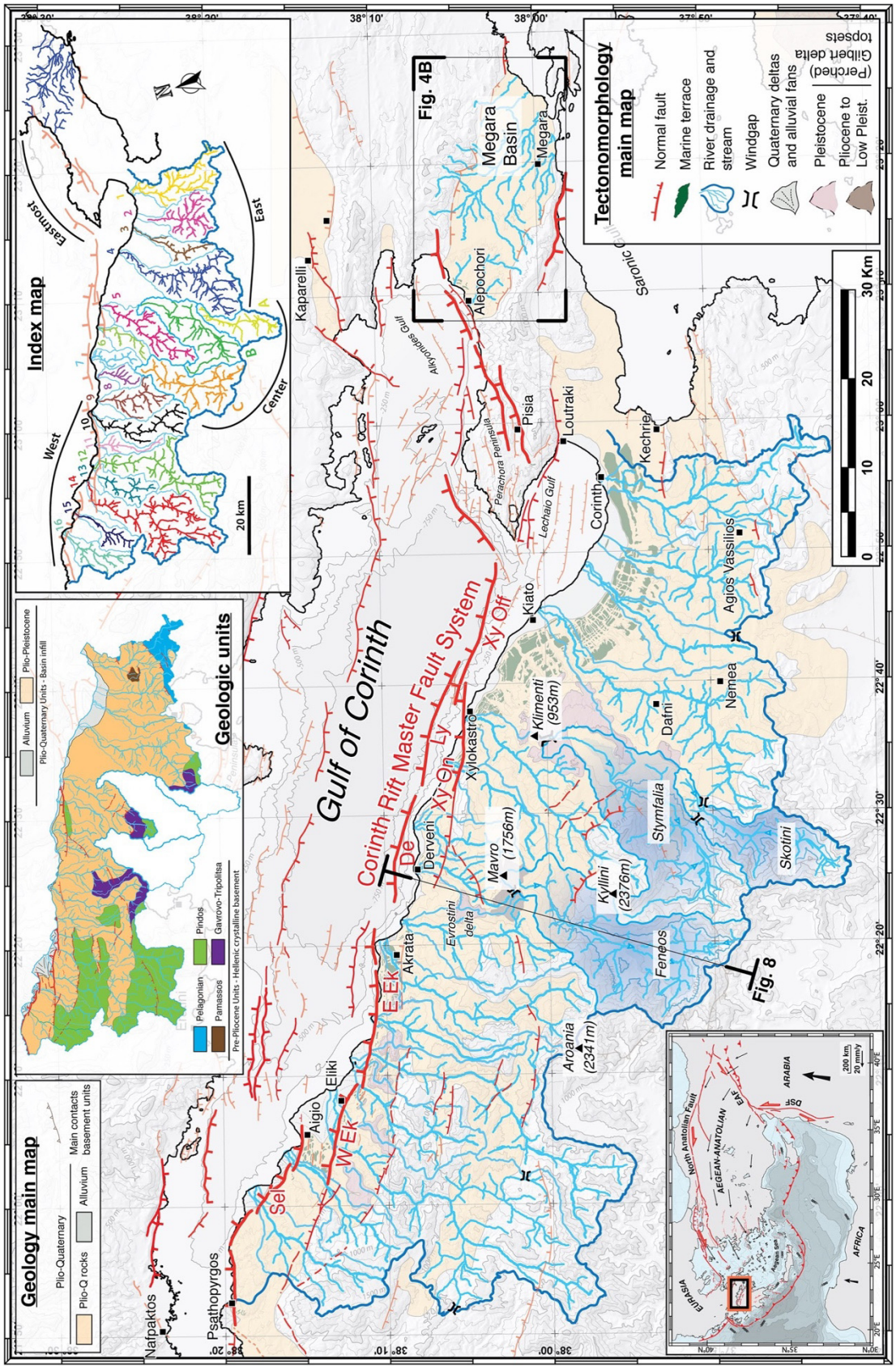
Geology main map
Plio-Quaternary
Alluvium
Main contacts basement units
Plio-Q rocks
Geologic units
Alluvium
Plio-Pleistocene
Plio-Quaternary Units - Basin infill
Pre-Pliocene Units - Hellenic crystalline basement
Pindos
Gavrovo-Tripolitsa
Pelagonian
Pamassos
Index map
Eastmost
East
Center
West
20 km
Tectonomorphology main map
Normal fault
Marine terrace
River drainage and stream
Windgap
Quaternary deltas and alluvial fans
Pleistocene
Pliocene to Low Pleist.
(Perched) Gilbert delta topsets
0
10
20
30 Km
Gulf of Corinth
Corinth Rift Master Fault System
Sel
W-Ek
E-Ek
De
Xy-On
Ly
Xy-Off
Fig. 4B
Fig. 8
Megara Basin
Megara
Alepochori
Kaparelli
Aliki
Eliki
Aigio
Akrata
Derveni
Xylokastro
Evrostini delta
Mavro (1756m)
Klimenti (953m)
Kyllini (2376m)
Aroania (2341m)
Fenéos
Stymfalia
Skotini
Dafni
Nemea
Agios Vassilios
Kiato
Corinth
Loutraki
Pisia
Perachora Peninsula
Lechaio Gulf
Kechries
Saronic Gulf
Nafpaktos
Psathopyrgos
ARABIA
AFRICA
EURASIA
AEGEAN-ANATOLIAN
North Anatolian Fault
DSF
EAF
200 km
20 mm/y

Figure 1

2. The modern Corinth Rift, its master fault system and footwall catchments

A basin-wide tectonic-induced unconformity and a concomitant distinctive shift in sedimentation, both onland (e.g., Ori, 1989) and offshore (e.g., Sachpazi et al., 2003), suggest that the onset of the modern (<1Ma) Corinth Rift occurred in relation to a recent, abrupt change in plate boundary conditions, imposed by propagation of the North Anatolian Fault into the Aegean (Armijo et al., 1996). This tectonic shift resulted in strain localization along major steep normal faults and the present high-amplitude relief. Many lines of evidence in the master fault footwall support this idea; (1) Plio-Pleistocene deltas are perched as high as ~1750 m just ~10 km away from the coast (e.g., Seger and Alexander, 2009); (2) abandoned paleosurfaces and paleochannels (e.g., Rohais et al., 2007); (3) river drainage reversals during Middle and Late Pleistocene (e.g., Dufaure, 1977); and (4) a flight of uplifted Quaternary marine terraces as old as 325 ka are found at ~400 m elevation barely 4 km from the present shore (Armijo et al., 1996).

Several WNW-ESE extensional fault segments that have surface lengths of ~10-25 km and dip northwards between 45º and 60º define the rift master fault system (Fig. 1). Elastic flexure (elastic-plastic flexure (s.s.), given the inelastic strain above the brittle-ductile transition and plastic strain below it) along these active rift-bounding faults regulate the modern architecture of the rift. That is, flexural footwall uplift and counteracting hanging wall subsidence maintain a structural relief >5 km and lead to extensive flights of marine terraces along the coast (e.g., Armijo et al., 1996; McNeill and Collier, 2004) (Fig. 1) and the growth of prominent syntectonic sedimentary wedges in the basin (e.g., Bell et al., 2009; Taylor et al., 2011). The master fault system cross-cuts older Hellenic units and normal faults that bound Plio-Pleistocene marine rocks, now exposed onland due to footwall uplift along the active faults (e.g., Collier et al., 1992) (Fig. 1). Since 350 ka, master fault segments in the centre of the rift, including the Xylokastro Fault and probably the Derveni and Lykoporia faults (Fig. 1), have sustained slip rates of 6-11 $mm \times yr^{-1}$ and rates of footwall uplift measured at several kilometers south of the master fault are in excess of 1 $mm \times yr^{-1}$ (e.g., Armijo et al., 1996). The rift-scale observation that ~65 % of the modern basin infill is younger than ~620 ka suggests low fault activity early on and an increase in basin infill rates initiating

between ~530 ka and ~340 ka, in agreement with increased fault activity at that time (Nixon et al., 2016).

Several river catchments drain the southern shoulder of the Corinth Rift, running northwards from the mountain range to the gulf (Fig. 1). These river catchments are roughly parallel to each other and drain approximately perpendicular to the rift-bounding fault system suggesting that they have the potential to maintain information regarding the evolution of the rift master fault along strike. In the centre of the Corinth Rift windgaps carved in south-tilted Middle Pleistocene rocks of deltaic conglomeratic systems (e.g., Dufaure, 1977) set the boundary between two formerly connected catchments (e.g., Seger and Alexander, 2009). While in the south, the sedimentary plains of Feneos, Stymfalia and Skotini are large flat-laying areas with internal drainage and gentle south tilt, in the north, steep short rivers drain northwards to the gulf. This implies drainage reversal at large scale (e.g., Dufaure, 1977), which has been proposed to result from rapid, sudden footwall flexural uplift of the master fault system (Armijo et al., 1996). Westwards of the reversed drainages, river morphology of the largest catchments is similar yet less marked, i.e. steep gorges and narrow valleys in a broad up-warped zone (e.g. knickpoint) separate a low-gradient low-relief upstream landscape from a steeper, higher relief landscape downstream (e.g., Seger and Alexander, 2009). East of the reversed drainages, dendritic upper river systems drain into narrow lower reaches without a clear intervening knickzone (e.g., Seger and Alexander, 2009).

3. Methods & conceptual framework

3.1. River profile analysis

Empirical research shows that in rivers where erosion and uplift are balanced, erosion rate increases monotonically with river channel steepness (e.g., DiBiase and Whipple, 2011; Kirby and Whipple, 2001, 2012; Wobus et al., 2006). Such observations imply a link between landscape morphology, erosion and rock uplift and provide the foundation for stream profile analysis. Moreover, the stream power incision model, i.e. quasi-physical expressions of detachment-limited river incision into bedrock, can be used to demonstrate that river channel steepness is sensitive to the ratio of erosion (or uplift) rate to substrate

erodibility, which is dictated by factors like lithology and climate (e.g., Kirby and Whipple, 2012; Snyder et al., 2000; Wobus et al., 2006). A convenient approach to analyze river profiles is through χ, a transformed distance coordinate defined as (Perron and Royden, 2013):

$$\chi = \int_{x_b}^{x} \left(\frac{A_o}{A(x)}\right)^{m/n} dx \quad (1)$$

where x is distance, A_o is a reference drainage area (here 1 m^2), A is upstream drainage area and m and n are positive constants. Here we use an m to n ratio of 0.45. Plots of χ versus elevation, referred to as a χ-plots, linearize river profiles by removing the influence of drainage area on the profile geometry (Perron and Royden, 2013). The slope of the χ-plot is the normalized steepness index (k_{sn}). Based on theoretical considerations, k_{sn} represents the ratio of erosion rate to erodibility raised to some power and is commonly used to assess relative changes in erosion or rock uplift rate in space and time (e.g., Kirby and Whipple, 2012; Wobus et al., 2006). See Suppl. material A for details.

Under the assumption that χ is a proxy for the theoretical steady-state elevation of a river network, χ-maps can be a useful manner to evaluate the present dynamic state of river basins (Willett et al., 2014). At equilibrium, steady-state channel head elevations should be the same. If not at equilibrium, a drainage divide migrates towards lower χ-values catchments until equilibrium is attained between both rivers, i.e. when channel head elevations across the divide reach similar χ-values (Willett et al., 2014).

Changes in relative base level or uplift rate lead to variations in river profile steepness that, under detachment-limited conditions, will propagate upstream as a kinematic-wave (Rosenbloom and Anderson, 1994; Whipple and Tucker, 1999). In the case of an increase in uplift rate, river profiles will steepen and a knickpoint (inflection point) will migrate upstream. While migrating, knickpoints bound gentler upstream channel reaches unaware of the change in boundary conditions from downstream, steeper channel reaches that are adjusted or adjusting to the change (e.g., Snyder et al., 2000; Whipple and Tucker, 1999).

3.2. Conceptual model of river response to normal fault footwall flexural uplift

An overall proportional relationship exists between normal fault maximum displacement (Dmax) and fault length (L) that, under unconfined mechanical conditions, results in fault displacement maxima at the center of the fault length and zero at its tips (e.g., Cowie and Scholz, 1992c; Dawers and Anders, 1995). This scaling sets footwall relief maxima at predictable distances from their active normal faults (e.g., Densmore et al., 2004), and controls the catchment area of footwall rivers (see Cowie 2006 for a complete overview). Since river longitudinal profiles are sensitive recorders of tectonic activity they can be used to reconstruct uplift histories in space and time (e.g., Gallen and Wegmann, 2017; Kirby and Whipple, 2012; Wobus et al., 2006). In fact, transient footwall rivers respond to changes in tectonic uplift rate developing long-profile convexities which height scales with the magnitude of the uplift rate increase on the fault (Whittaker et al., 2008). Thus, longitudinal and χ profiles of footwall catchments laying orthogonally along the strike of their active faults, i.e. along the direction of maximum variation in flexural uplift signal, should allow for an accurate description of footwall elastic flexure.

We attain a simple approximation of longitudinal and χ profiles of flexed normal fault footwall catchments running orthogonally to fault strike by means of a detachment limited stream power incision model (Fig. 2 and Suppl. material B). This model is designed only to illustrate the general expected behavior of a footwall river in response to initiation of rapid flexural uplift and is not intended to be specifically representative of the Corinth Rift rivers. Therefore, its results can be regarded as conceptual for the purposes of this study only. An imposed signal of flexural uplift decaying exponentially away from the fault trace results in the formation of a broad convexity, or knickzone, in river longitudinal and χ profiles (Fig. 2). This knickzone is defined by a steep convex-upwards lower reach and a flat reach directly upstream. As time progresses the convex lower reach grows as the knickpoint migrates upstream until profile recovery (Fig. 2). Similarly, the flat region immediately upstream of the knickpoint expands until it reaches the top of the profile and is ultimately consumed by the knickpoint. During the transient phase, erosion rates above the knickpoint drop to zero and deposition must take place in the channel to

maintain continuity of the river network (Fig. 2). If the vertical celerity of the knickpoint outpaces the rate of sedimentation in the upper reach, drainage reversal will occur. This makes the upper reaches susceptible to reversal in footwalls responding to rapid fault slip rates through elastic flexure.

Fig. 2. A) Theoretical χ-plots in relation to scenarios of a tectonically controlled landscape. In panel A, χ-plots in steady state in the left and χ-plots of transient response to footwall flexural uplift. Small insets in the upper left are conceptual representation of vertical tectonic motions related to each χ-plot. B) Model of response of river profile to rapid flexural uplift assuming the detachment limited stream power incision (see Suppl. material B for details).

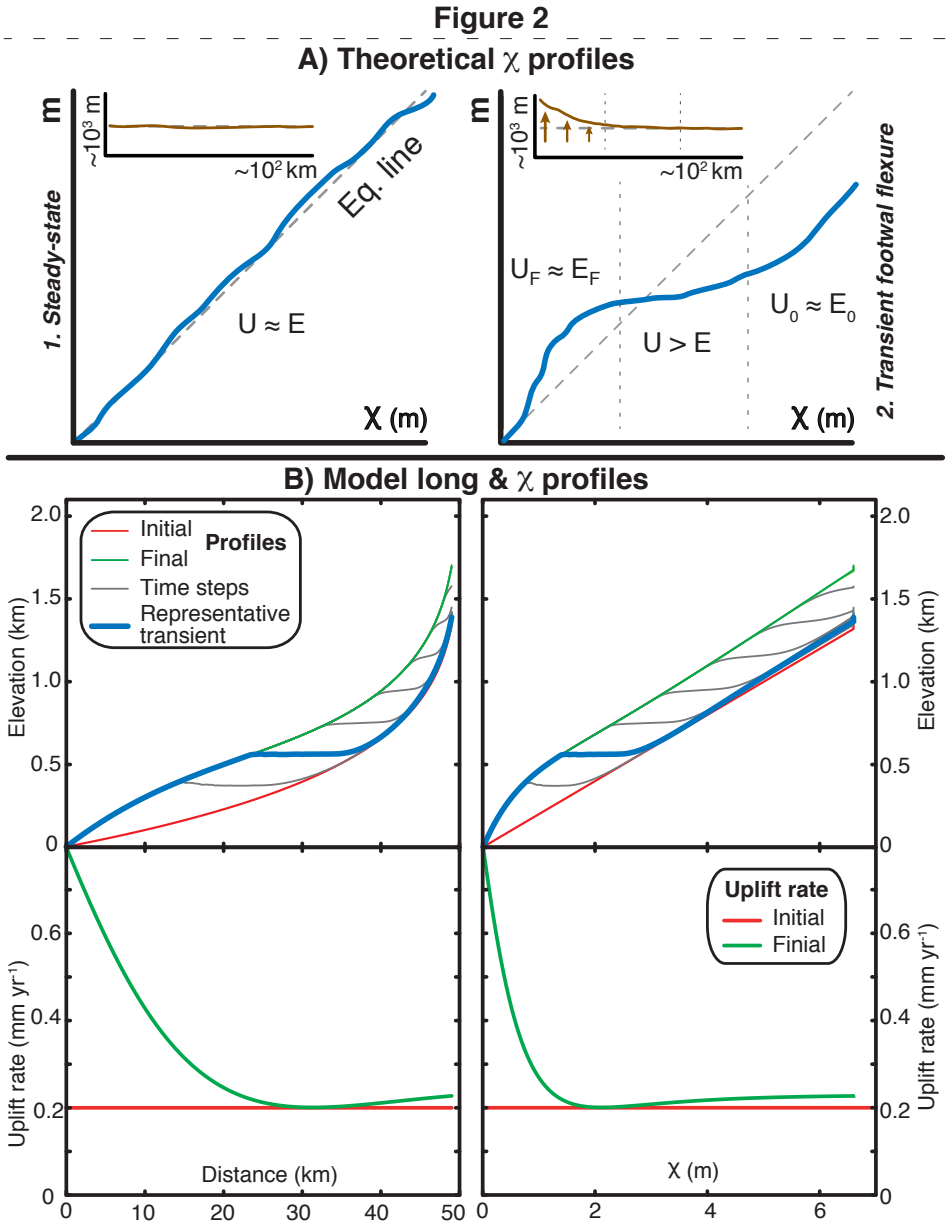

3.3. Focus, procedures and specific corrections

We focus on the 16 largest catchments and 3 corresponding reversed rivers of the southern shoulder of the Corinth Rift, west of Perachora peninsula (Fig. 1). We assess the morphologic characteristics of these river networks as a function of their distance from and position along the master fault and in terms of spatiotemporal variations in footwall uplift rate. This analysis allows us to identify three distinct footwall sectors (see up-right inset in Fig. 1); "east", "central" and "west" (i.e. east of Kiato, from Kiato to Akrata, and from Akrata to Psathopyrgos, respectively). We also analyzed rivers in the rift easternmost sector, east of Perachora peninsula (Fig. 1), to support specific arguments.

We use Topotoolbox 2.0 (Schwanghart and Scherler, 2014) to extract river profiles from the Digital Elevation Model (DEM), and the χ Profiler package (Gallen and Wegmann, 2017) to perform river profile analysis. We used a composite 20-m resolution DEM for the catchment area of gulf draining rivers and included the three largest reversed river basins that are now endorheic. We performed specific corrections to portray the river network morphology and longitudinal profiles of the endorheic basins that do not reach the regional base level by creating an artificial outlet, and plotting them according to their flow direction in nature. See Suppl. material A for details.

4. Results

4.1. Along-strike variations in longitudinal profiles

Longitudinal profiles of the 16 largest rivers draining the southern shoulder of the Corinth Rift show departures from smooth graded equilibrium profiles, under the assumption that rock uplift and substrate erodibility are uniform in space and time (Fig 3, Suppl. material C to R). Importantly, variations in river profile geometry away from a theoretically steady-state profile are systematic and a function of catchment location along master fault strike, allowing us to classify them into three distinct groups, as previous workers did on the basis of plain-view river morphology (e.g., Seger and Alexander, 1993). For

simplicity, we have selected the Asopos (4), Dervenios (8), and Vouraikos (12) rivers as representatives of each of these groups (cf. Suppl. material C to R).

4.1.1. Eastern river catchments

In the east, footwall river basins cover large areas of low topography and discharge into the Lechaio Gulf, in the footwall of the master fault. The master fault departures from the coast eastwards at an angle and turn to a NE-SW orientation, setting the northern coast of the Perachora Peninsula (Fig. 1). Longitudinal profiles (1 to 4, Fig. 3) are markedly flat (<300 m elevation in >15 km) and show a broad low-angle bend downstream at mid elevations in all cases but for Raizanis River (2, Fig. 3). River profiles show modest departures of an equilibrium profile, assuming spatially and temporally uniform uplift and erodibility, and grade eastwards into the expected concave upwards profiles of steady-state rivers (1 to 4, Fig. 3). The position and orientation of the master fault influences the areal extent of river catchments; the drainage of the Asopos River (4, Fig. 3), at a western position within the east rift, is of similar size (~250 km^2) to those of the internally drained basins to its west (C and B-A, Fig. 3) but notably smaller catchments exist farther east.

4.1.2. Central river catchments

In the centre of the footwall of the Corinth Rift, steep exorheic rivers close to the coast drain the highest relief portions of the footwall and flat-laying endorheic rivers occupy the high elevation landscape farther inland (5 to 9 and A to C, Fig. 3). The shortest and steepest river networks (6 to 8, Fig. 3) are located at the front of the reversed drainages (A to C, Fig. 3) and between larger rivers (5 and 9, Fig. 3). Taken together, these rivers show the largest departures from an inferred steady state profile geometry (Fig. 3). The drainage divide of the short and steep rivers flowing to the gulf (6 to 8, Fig. 3), with the headwards at >1 km elevation at <15 km of their outlets, is two times closer to the shore that elsewhere in the rift (Figs. 1 and 3). These steep exorheic rivers share a drainage divide with the extensive (~40 km) elevated (>700 m) low-relief endorheic basins to the south. The perched paleo-deltas of Mavro (1756 m) and Klimenti (~950 m) lie along these drainage divides and their topsets are carved by dry valleys and windgaps

(Rohais et al, 2007). These reversed drainages drain internally the extensive plains of Feneos, Stymfalia and Skotini (A, B and C in lower inset of Fig. 3-A) and tend to exhibit dendritic drainages.

4.1.3. Western river catchments

Rivers in the western rift (10 to 16, Fig. 3), where the master fault outcrops onland leading to an area of elevated topography, exhibit a broad upwarping at distances close to their outlets (Fig. 3). In the west, rivers lengths are variable, alternating between short (<15 km) and long (≥35 km) with the exception of the westernmost drainage basin, Finikas (16 in Fig. 3, Suppl. material R). While the short rivers are uniformly steep, having morphologies similar to the steep gulf draining rivers of the central rift, the long rivers systematically decline in steepness westwards. Furthermore, the long rivers have broad knickpoints that separate steep downstream reaches carved in deep gorges from wide flat upstream reaches (see also Seger and Alexander, 2009). This characteristic morphology is best exemplified by the Vouraikos River (12, Fig. 3).

Fig. 3. A) Representation in map and longitudinal profile view of the eight largest river networks draining the southern coast of the Corinth Rift, and the three internally drained river basins of Feneos, Stymfalia and Skotini. Each river is represented at the same scale, and with a vertical exaggeration of ~4,5 in their longitudinal profiles. We followed a color code to relate the plain and longitudinal views of each river network. B) Overarching characteristics of river networks as seen in their longitudinal profiles and map views, as per rift sector; east - Asopos (4), centre - Dervenios (8)/Olvios (C), and west - Vouraikos (12) of the rift.

Figure 3

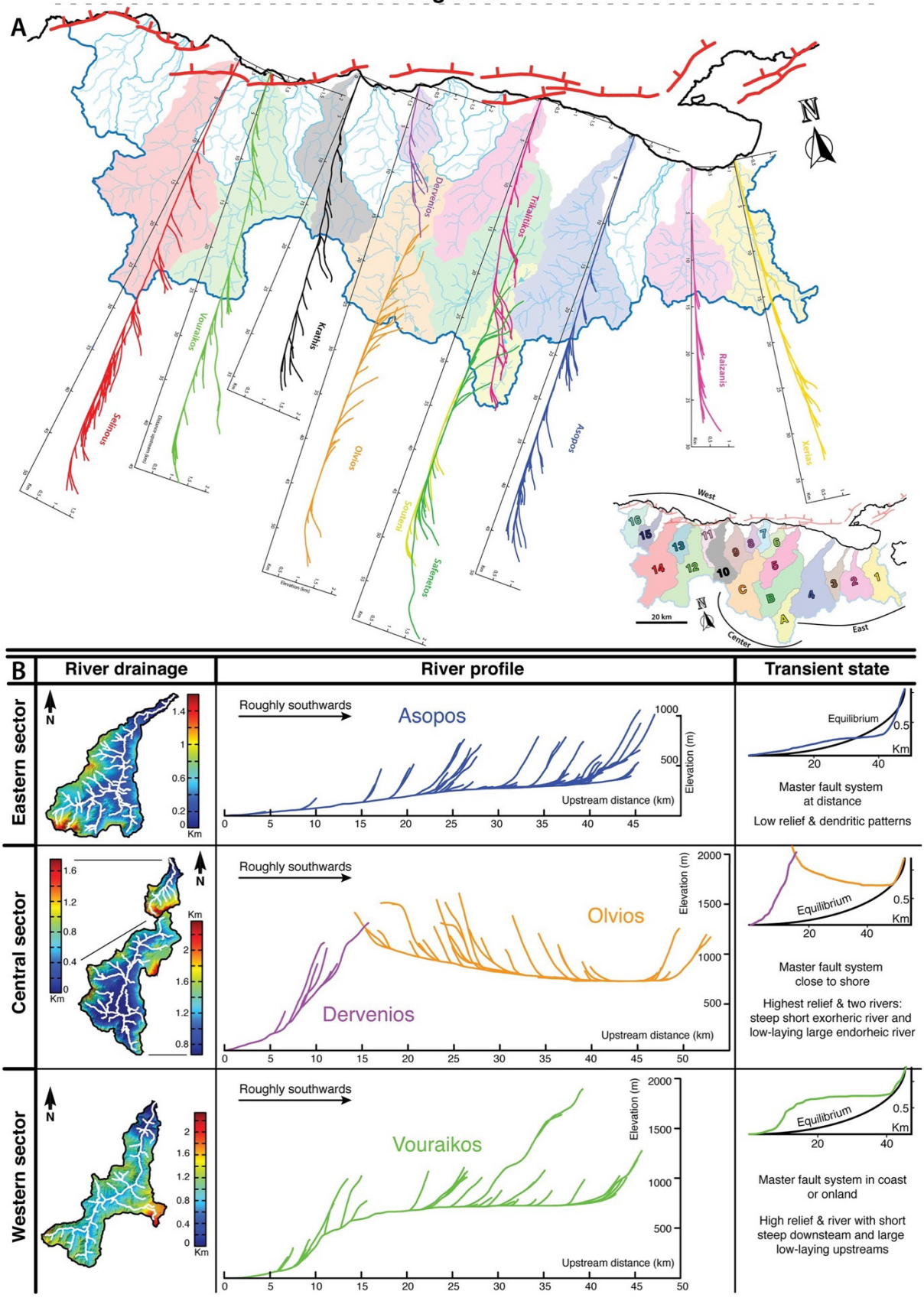
A
Selinous
Vouraikos
Kerynitis
Olvios
Souteni
Sideretos
Asopos
Dervenios
Trikalinikos
Raizanis
Xerias
N
West
Center
East
20 km
B
River drainage
River profile
Transient state
Eastern sector
Central sector
Western sector
Roughly southwards
Asopos
Olvios
Dervenios
Vouraikos
Upstream distance (km)
Elevation (m)
Km
Equilibrium
Master fault system at distance
Low relief & dendritic patterns
Master fault system close to shore
Highest relief & two rivers: steep short exorheic river and low-laying large endorheic river
Master fault system in coast or onland
High relief & river with short steep downsteam and large low-laying upstreams

4.2. Reversed rivers in the Corinth Rift

The Corinth Rift main shoulder provides an outstanding example of reversed drainages, a relevant feature in continental rifts that has been studied both by field studies and numerical modelling (e.g., Armijo et al., 1986; Cowie et al., 2006). Here, we first describe the process in the easternmost rift, where a simpler catchment adjustment to a similar driving mechanism can be traced at present by means of fluvial metrics. Then, we use this analog to describe the prominent drainage reversal observed in the rift centre.

4.2.1. Easternmost rivers

In the Pliocene-to-Quaternary marine rocks of the Megara Basin, a low elevation (~250 m) drainage divide runs roughly N-S <10 km southeast of the ENE-WSW-striking master fault (Figs. 1 and 4-A,-B). The tributaries of rivers reaching both sides of this divide exhibit "barbed" planview geometries, i.e. right angle kinks change river flow from roughly coast-parallel to coast-perpendicular (Fig. 4-B). Longitudinal profiles lie at low elevations at both sides of the divide, but rivers facing the main fault are markedly shorter (Fig. 4-A). A sharp contrast in χ-values across this divide is also observed (Fig. 4-B). Collectively, this evidence suggests ongoing drainage reorganization and southeastwards divide migration in relation to the presently active normal fault.

4.2.2. Central rivers

As discussed above, three endorheic basins lie south of the steep gulf draining rivers in the centre of the rift and windgaps are observed along their common divide at ~15 km from the master fault (Fig. 1). Windgap orientation suggests that the lower reaches of Trikalitikos River (5) and the Dervenios River (8) correlate with the reversed rivers of Safenetos (B) and Olvios (C), respectively (Figs. 1, 3 & 4). The latter is connected to the Souteni River (A), which is not clearly linked with the gulf draining rivers. The trunk channel in all three reversed basins has a similar, generally concave upwards geometry, with an extensive flat interior increasing in slope towards both ends (Fig. 4-C,-D). These large flat surfaces are slightly tilted southwards and at higher elevation to the west; the eastern plain (A) lays ~75 m lower than the

central equivalent (B), which is in turn ~75 m lower than the Olvios stream of Feneos (C), at ~725 m (Fig. 4-C,-D). Their respective windgaps are carved on rocks that are progressively older (Ford et al., 2016) and lay at higher elevations westwards; on the topsets of the Middle-Late Pleistocene Klimenti Delta at ~950 m, and on those of the Late Pliocene - Early Pleistocene Mavro Delta at ~1300 m. It follows that reversal of these river systems progressed from west to east within the central rift sector. However, the longitudinal profiles of the reversed Safenetos (B) and Olvios (C) rivers contain two sets of convex upwards inflexions (knickpoints) at their north and south ends that occur at roughly the same elevation in both rivers, ~1100-1200 m and ~1350-1450 m (Fig. 4-C,-D). Taken together, these evidences suggest that the reversed rivers show a common early evolution and later diachronic reversal.

Fig. 4. Corinth Rift rivers showing first-order reversals and the neoformation of drainage divides in relation with the activity of the modern system of normal faults. A) and B) are the χ-map of the main rivers flowing in the Megara basin and the longitudinal profiles of the largest network on each side of the new divide. The χ-map in panel B is set as an homologous for the other two cases, panels C) and D), for which the production of such map is challenged by the absence of common base level. C) and D) are the longitudinal profiles of the reversed river networks and their corresponding exorheic rivers. C) for Souteni (A)/Safenetos (B) - Trikalitikos (5), and D) for Olvios (C) - Dervenios (8). Knickpoints in the internal basins are marked with red stars.

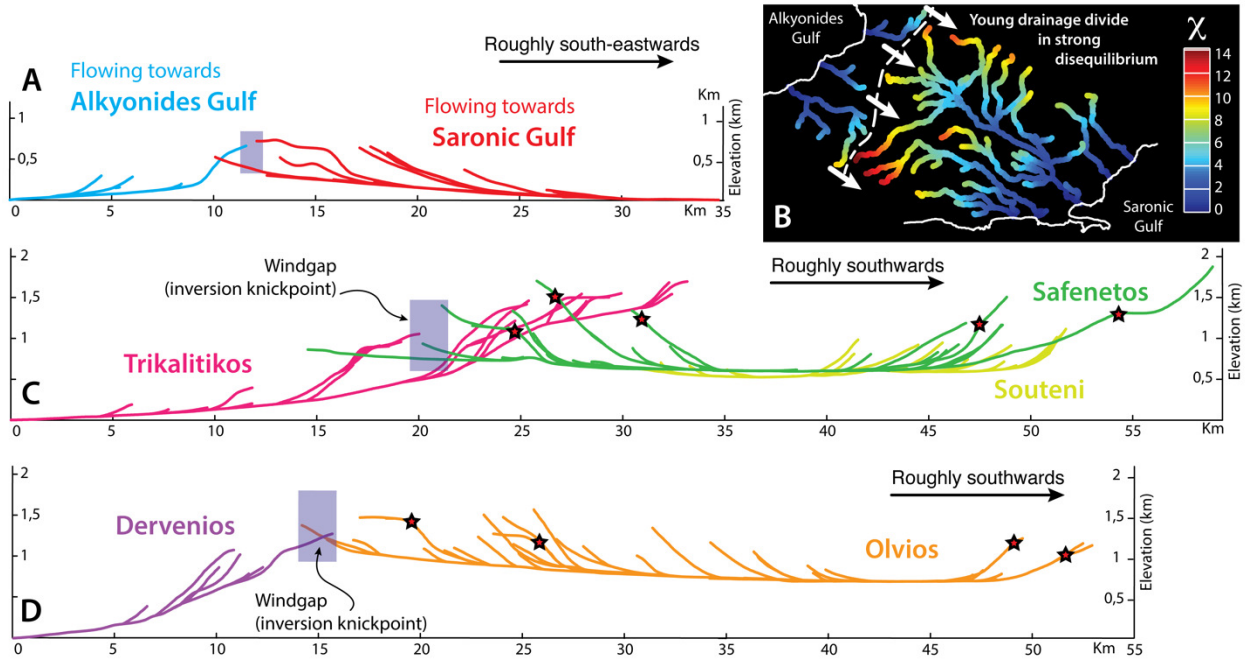

4.3. χ-plots and k_{sn} of gulf draining rivers

Consistent with above, χ-transformed river profiles fall into three broad classifications related to the east, central and western rift domains that we show as per their representative networks (Fig. 5). χ-profiles in the east (Fig. 5-A and Suppl. material F) lay low and have one broad, low-elevation (~250 m) knickpoint separating a steep lower reach from a shallow upper reach, before gaining elevation further upstream. Basin average normalized steepness index is the lowest of all three sectors (Fig. 5-B). In the central sector, χ-profiles are uniformly steep and linear with no obvious broad knickpoint and exhibit the highest basin average k_{sn} (Fig. 5 and Suppl. material J). The western sector χ-profiles have broad, prominent knickpoints at ~700 m that separate steep lower reaches from gentler upper reaches, steepening at the uppermost reaches. Basin average k_{sn} falls between that of the eastern and central sectors (Fig. 5 and Suppl. material N). These primary trends can also be seen in all 16 river networks analyzed (Suppl. material C to R). Similar morphologies appear for rivers near our chosen "representatives", and a stepwise along-strike transitional χ-profile morphologies lie between them, with two exceptions: from Asopos (4) to Trikalitikos (5) in relation to larger distances between the master fault and the coast, and from Selenious (14) to Meganitis (15), in relation to a jump in the master fault system (Suppl. material C to R).

Fig. 5. χ-plots of representative rivers of each rift sector at a similar scale (east - Asopos (4) in blue, centre - Dervenios (8) in purple and west - Vouraikos (12) in green). χ-profiles have a broad knickzone at low elevations in the east, are uniformly steep and linear in the centre and have a wide prominent knickzone at high elevations in the west.

Figure 5

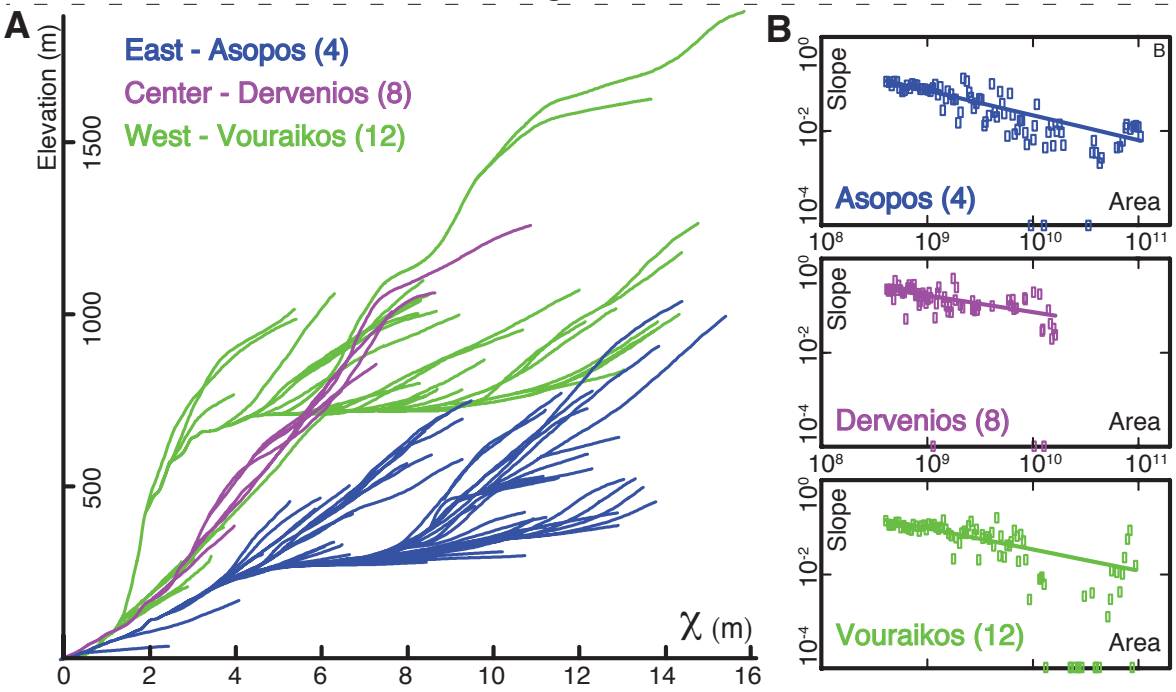

4.4. Normalized steepness index (k_{sn}) map

We built a normalized steepness index (k_{sn}) map to evaluate the ratio of uplift rate to bedrock erodibility (Fig. 6). Fig. 6-A shows k_{sn} values in three groups (k_{sn} < 300 $m^{0.9}$ in blue, 300 > k_{sn} > 450 $m^{0.9}$ in orange and k_{sn} > 450 $m^{0.9}$ in purple) and the inset map (Fig. 6-B) highlights regional trends of the last two groups. In the east, k_{sn} values are markedly low for rivers 1 to 3, completely absent of k_{sn} values > 300 $m^{0.9}$ (Fig. 6-B). Westwards, the cluster with highest channel steepness (k_{sn} > 450 $m^{0.9}$, reaching values of ca. 950 $m^{0.9}$, purple in Fig. 6-B) follow a linear stripe parallel to the main fault approximately from the western tip of the Xylokastro Onshore Fault to the western tip of Western Eliki Fault. The second trend of high steepness, 300 > k_{sn} > 450 $m^{0.9}$ (orange in Fig. 6-B), has also a broadly linear shape, and lays at positions farther away from the main active fault, and between the reversed drainages in the Trikalitikos River (5), and the Asopos River (4). The swath of elevated k_{sn} values pass through several lithologic contacts while remaining laterally continuous (cf. Fig. 1) and have overall parallel trends along master fault strike, which suggest a genetic relationship with the master fault system rather than features associated with canges in substrate erodibility.

Fig. 6. Normalized steep index (k_{sn}) map of the topography related with drainages that outlet in the southern shoulder of the Gulf of Corinth. We used a θ_{ref} = 0.45, for channel network segments of 500 m at >1 km from the divide and a smoothing window of 500 m for both maps. For map A, we show 3 groups of k_{sn} values, k_{sn} < 300 in blue, 300 > k_{sn} > 450 in orange, k_{sn} > 450 in red. In map B we manually draw the envelopes that enclose k_{sn} groups with overall values of 300 > k_{sn} > 450 (in orange), k_{sn} > 450 (in red).

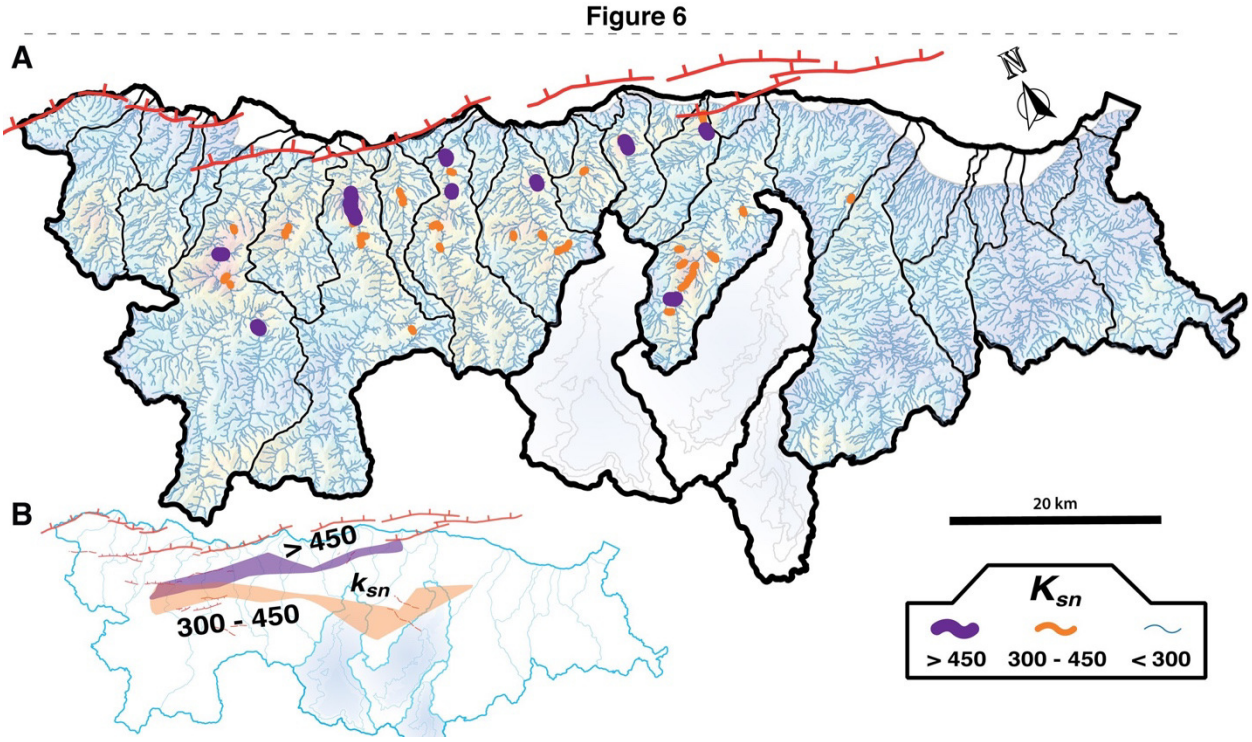

5. Discussion: Relief response to evolution of the Corinth Rift master fault

The relatively uniform climate in the Corinth Rift main shoulder suggests that it has little effect on the observed along-rift landscape variability (Karymbalis et al., 2016a); however, lithology varies in the study area (Fig. 1). Plio-Pleistocene infill rocks, composed of coarse-grained continental, shallow marine marls, and non-marine limestones, unconformably overlay Hellenic Units crystalline rocks, mostly phyllites, schists, quartzites and metalimestones (Gawthorpe et al., 2017) (up-centre inlet of Fig. 1). Eastern rivers almost entirely incise syn-rift rocks but central and western rivers carve also the more resistant crystalline rocks in their middle and headwater reaches (Fig. 1). Given these major differences in rock-type, it is important to evaluate the role of changes in the pattern of bedrock erodibility on our analysis. For example, the normalized steepness index (k_{sn}) (section 4.4) is a function of bedrock erodibility; all else

being equal, rivers incising more erodible rocks will have lower steepness relatively to less erodible units. Low steepness values in the eastern portion of the rift correspond to wide expanses of sedimentary rocks interpreted to be less erodible (Fig. 6). However, as these eastern rivers are farther from the active fault trace, it is likely that the lower steepness also reflects lower rock uplift rates. To the west, the steepest river reaches are found along the coast line and k_{sn} is relatively lower upstream in these basins (Figs. 5 and 6). This relative pattern in k_{sn} is the exact opposite pattern one would expect if uplift were uniform and erodibility were the dominant factor controlling k_{sn}. For these reasons, we are confident that changes in bedrock erodibility plays a an important, but subsidiary role on river profile morphology, and that the spatiotemporal patterns of rock uplift imposed by the Corinth Rift active fault system is the dominant factor controlling spatial patterns of k_{sn} and thus river morphology.

5.1. River response to fault initiation and flexural uplift

For the following discussion, we consider former single catchments in the rift centre as individual elements despite their present disruption into exorheic and endorheic rivers (5 to 9, B and C) (Fig. 4, C and D). A stark transition in morphology and geometry of river systems is observed in ~15-25 km from the master fault along its strike. This transition is marked as a major convex inflexion in the river profiles (i.e. a major knickpoint or a windgap) that separate steep lower reaches, or gulf draining rivers, from low gradient uplands reaches, or endorheic basins (Figs. 1, 3, 4 & 5). The position of the major inflexion and the magnitude of related river channel steepening vary consistently along the master fault strike. Knickpoints are at relatively farther distances from the master fault in the east, windgaps lie the closest to it in the centre, and major knickpoints are at intermediate locations yet are still close to the master fault in the west (Figs. 1, 3 and 4). The magnitude of river channel steepening is more limited in the east rift, maximum in the centre, and intermediate yet high in the west (Fig. 3). Lateral transitions of both the major inflexions and the channel steepening are gradual along the master fault strike, except where *(i)* the master fault gains distance from the coast in the east and *(ii)* has a jump on its trace in the west (Suppl. material C to R). We interpret the consistent variation of the major inflexion and the magnitude of river

channel steepening along the master fault strike as reflecting a change in footwall flexure amplitude (e.g. more rapid uplift) along the rift southern shoulder.

River profiles exhibit a swath of high k_{sn} values that is parallel to the master fault in reaches below windgaps and knickpoints in the central and western rift sectors, respectively (Fig. 6). This is consistent with previous studies that demonstrate fault slip rates of 4-11 mm×yr^{-1} over the past ~330 ka in these rift sectors (Armijo et al., 1996; McNeill and Collier, 2004). Collectively, these evidences indicate that windgaps and main knickpoints along the Corinth Rift southern shoulder are of common origin and suggest a temporal, drastic increase in uplift rate along the full length of the modern master fault system. In the western and eastern sectors, χ-profiles of large footwall rivers have a sigmoidal shape with a steep lower reach and a low gradient upper reach separated by a knickpoint (Fig. 5, Suppl. material C to G and K to R). In the central sector, the steep χ-profile corresponds to beheaded rivers to the north of low gradient endorheic basins (Fig. 5, Suppl. material H to J). Both morphologies are well explained by an across strike pattern of uplift consistent with rapid mechanical unloading and flexure of a normal fault footwall (Fig. 2).

A rapid increase in flexural uplift of a normal fault footwall generates a knickpoint, in both longitudinal and χ river profiles with a broad sigmoidal shape (Fig. 2), as observed in the eastern and western sectors (Fig. 5). This profile morphology develops in large rivers eroding flexing footwalls of normal faults with moderate or high slip rates (e.g., Vouraikos, 12), even at a certain distance from the fault (e.g., Asopos, 4). Other, relatively short transient rivers developing in flexed footwalls only experience a small across strike gradient in uplift rate. As such, their morphologies show little to no influence of the exponential headwards decline in rock uplift rates associated to their normal faults (Zapantis and Kerinitis, 3 and 13 in Fig. 1, and Suppl. material C and K). If flexural uplift is rapid enough, sediment will be deposited in the river reach above the newly formed knickpoint as the upper reaches are back-tilted. If deposition rates cannot keep pace with downstream rock uplift rates, rivers will be beheaded from their upper reaches (e.g., Cowie et al., 2006). This latter scenario occurs in the central

Corinth Rift, where lower reaches become rivers that maintain a steep longitudinal and χ profiles reflecting the current coastal uplift rate (e.g., Dervenios, 8), and the corresponding upper reaches become a reversed drainage where we lose the capacity to track fluvial metrics (e.g., Olvios, A).

Aforementioned evidence suggest that drainage reversal in the central sector of the rift represents an extreme setting of footwall flexure and a radical increase in uplift rates caused by a change in fault slip rate. The timing of the change in tectonic forcing that resulted in windgap formation and drainage reversal in the rift centre is uncertain. However, we infer that flexure was effective after deposition of the Evrostini delta, which Ford et al. (2016) sets as ~0.7 Ma, on the basis of the size of the Mavro and Evrostini deltas and the continuity between their windgaps.

Uplift rate acceleration due to motion along a new master fault system not only led to drainage reversal in the central sector, but also to the ongoing drainage network rearrangement observed to the west and east. In the west, variations in channel head χ-values observed in χ-maps indicate that large river drainages are presently expanding laterally in the upper reaches by capture of drainage area from adjacent basins (Fig. 7). In the east, behind the Lechaio Gulf, forced river drainage narrowing by incision of their downstream reaches occurred after land uplifted to the north of stable river catchments. In the Megara Basin farther east, barbed tributaries near a new drainage divide and strong contrast in χ along the divide demonstrate that coastal drainages are migrating headwards in response to the new master fault system (Fig. 4-B). This evidence shows that river networks not only adjust to changes in tectonic forcing by changing channel morphology (e.g., slope and width), but also geometrically reorganize in response to newly imposed boundary conditions.

Fig. 7. χ-map of upstream sectors of rivers in the east sector. White arrows indicate drainage divide migration direction. Two-level thickness represents different levels of disequilibrium, inferred from across-divide χ-values.

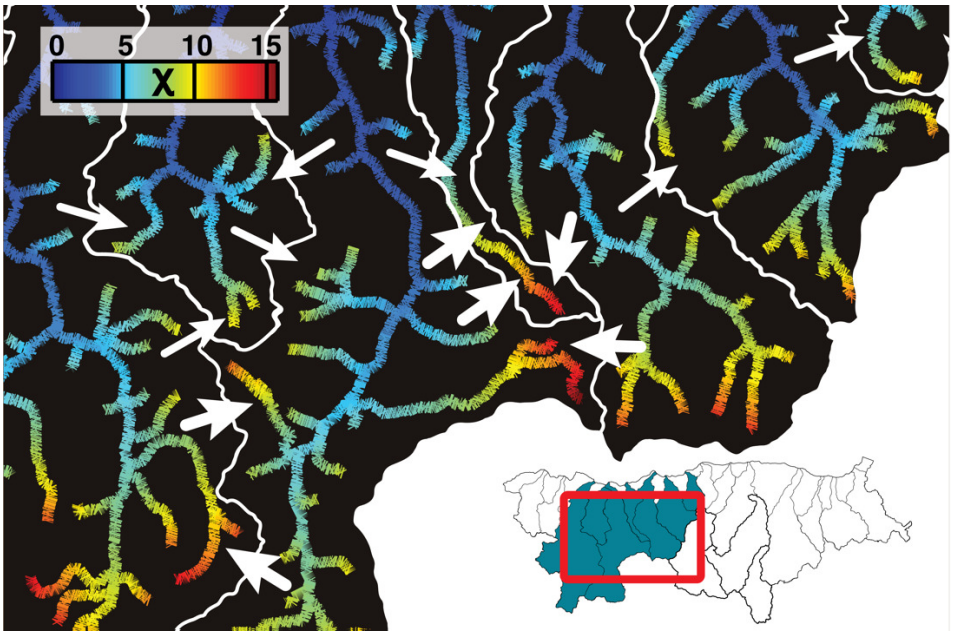

5.2. Mechanical and tectonic implications

As discussed above, footwall river morphologies and transient drainage reorganization in the southern shoulder of the Corinth Rift respond to fast onset of a new master fault system. Further, longitudinal river profiles report an asymmetry in flexure amplitude along master fault strike, with its maximum in the rift centre, and decaying laterally; gently to the west and sharply to the east. We associate such amplitude signal in footwall flexure of the normal fault system to its (along-strike) displacement profile. Given that displacement in normal faults is approximately proportional to their length (e.g., Cowie and Scholz, 1992c), and individual faults would show individualized local minima and maxima (e.g., Dawers and Anders, 1995), such ~100 km bell-shaped fault displacement profile implies that individual (at-surface) fault segments in the Corinth Rift southern shoulder are linked at depth in a single rift-scale master fault. This new master fault causes flexural uplift that was possibly effective <0.7 Ma (see above) in the rift center and continues today at the scale of the entire rift southern shoulder.

Fast slip rate change and asymmetric flexural response along the new master fault strike could be explained either as *(i)* a roughly coeval fault growth with different fault flexural uplift rates at different rift sectors, or as *(ii)* a time-transgressive fault growth with similar fault flexural uplift rates that initiated in the rift centre and propagated laterally. Estimated slip rates of the master fault system for the last ~330 ka cannot discriminate between both options, since estimates for the centre of the Corinth Rift (minimum of 6–7 mm×yr^{-1} and up to 11 mm×yr^{-1}; Armijo et al., 1996), and in the west (4–7 mm×yr^{-1}; McNeill and Collier, 2004) overlap within uncertainty. We favor time-transgressive fault growth on the basis of the consistently-high k_{sn} values, increasing westwards parallel to the master fault along its strike (Fig. 6), hence conveying a similar or west-increasing uplift rate in both rift sectors. Younger depocenter growth in the western rift (Nixon et al., 2016), chrono- and lithostratigraphy evidence (Ford et al., 2016), and the diachronous reversal of rivers basins shown here for the central rift (see section 4.2.2) strengthens this hypothesis. In the eastern rift, river morphologic response to flexure is masked by distance from the master fault.

We propose a conceptual model compatible with the aforementioned evidence and consistent with geologic observations in the central part of the Corinth Rift (Fig. 8). The model illustrates the evolution of river catchments under rapid footwall flexure. The model suggests the progressive step-by-step abandonment of a Gilbert delta fan sequence as the structural relief grows across the rift master fault (Fig. 8). Such relief growth ultimately stimulates large-scale drainage reversal and forced endorheism. In this conceptual model both fan delta abandonment and river drainage reversal are direct outcomes of strong fast normal fault flexural uplift.

Fig. 8. Conceptual time-evolution of Gilbert delta(s) and river profile(s) in the centre of the rift in relation to elastic flexure in the footwall of the master fault. Rough location of the section is shown in Fig. 1. Figure is not to scale in the horizontal and only roughly proportional in the vertical. Footwall flexural uplift is marked in dimmed colours. The upper profile correspond to the Early-Mid Pleistocene, and the bottom profile represent Modern times. In-between times steps were not specifically constrained, but can be roughly assigned to ~1 Ma, ~700 ka, ~300 ka and Present. Before initiation of activity in the master fault, the Dervenios-Olvios River fed the Mavro Gilbert Delta. Master fault activity initiation and subsequent footwall flexural uplift led Mavro Gilbert Delta abandonment and Evrostini Gilbert Delta deposition at younger times. Further footwall flexural uplift abandoned the Evrostini Gilbert Delta and eventually forced drainage disruption, and hence the differentiated rivers of Derenios (exorheic) and

Olvios (endorheic). We represent drainage reserval only in the last profile, but could have taken place anytime after ~700 ka (see main text). Both Gilbert deltas large size and prominent foresets (Seger and Alexander, 2009) suggest that Dervenios-Olivos was an extensive long lived catchment. Younger and modern underdeveloped Gilbert deltas (Karymbalis et al., 2016a; Rohais et al., 2007) develop in relation to the newly formed short and steep exorheic Dervenios River.

Figure 8

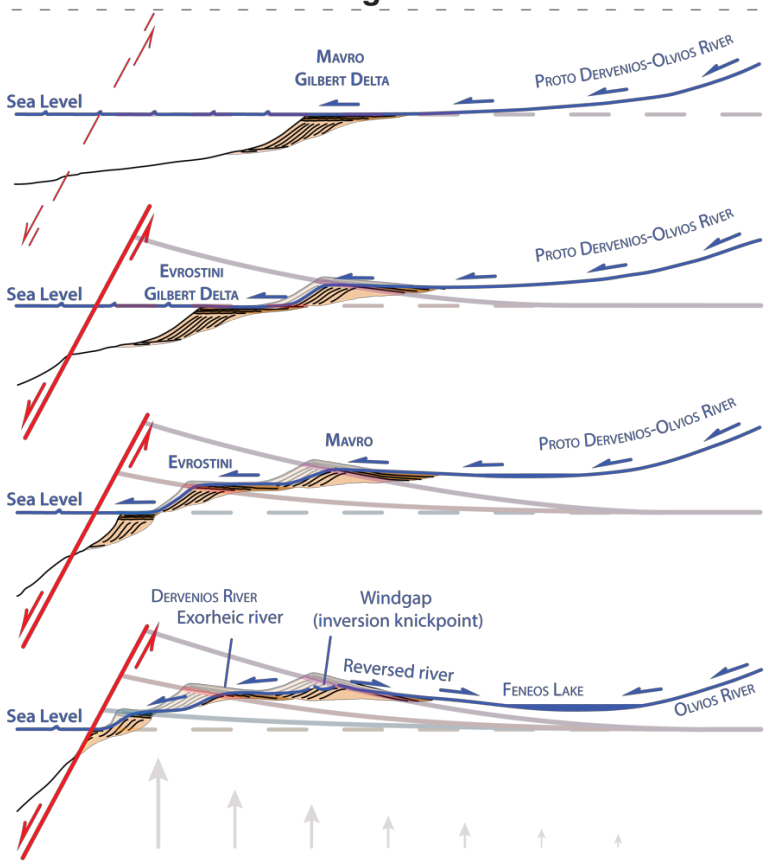

The elastic flexure and drainage reversal documented in this contribution report a fast footwall flexural uplift at rift-scale (extending for lateral lengths >100 km and resulting in structural reliefs >5 km) that is at odds with previous models of Corinth Rift growth. Models proposing that at-surface steep normal faults sole out into a shallow low-angle detachment dipping north (e.g., Rigo et al., 1996; Sorel, 2000; Jolivet et al., 2010) are incompatible with this evidence. These models would produce overall subsidence towards the present master fault, and not an increasing flexed uplift signal. Similarly, models that explain Gilbert deltas abandonment by progressive basinwards migration of rift-bounding faults (e.g., Ford et al., 2016, 2012; Goldsworthy and Jackson, 2001) are unable to account for the large-scale flexure and drainage reversal. In such "discrete rider block" models, with ~5-to-10 km tilted blocks (see Ford et

al., 2016, Figs. 3, 4; Gawthorpe et al., 2017, Fig. 2-b), the uplift rate linear decay due to their basinward-bounding faults results in "saw-tooth" river longitudinal profiles (Suppl. material S-1). Unless the length of the tilted block compares to the full length of the river (Suppl. material S-2), such linear decay in uplift rate leads to river profile morphologies inconsistent with the evidence (Suppl. material C to R). Given that the shape of marine terrace flights is compatible with elastic flexure (Armijo et al., 1996; de Gelder et al., 2017), we favor that uplift rate flexural decay occurs all along the main rift shoulder of the Corinth Rift, rather than in relation to the unlikely tilt of a ~100-km-along-strike, ~50-km-across-strike block.

As modeling efforts suggest, footwall uplift at significant scales (Resor and Pollard, 2012) and uplift-to-subsidence ratios of ~1:2–3 require steep faults that reach at least the brittle-ductile transition (Bell et al., 2017). High-angle planar faults seen at the surface (e.g., Bell et al., 2011; McNeill et al., 2005) reaching the brittle-ductile transition with equivalent dips (Bell et al., 2017) is therefore the most probable cause of such localized flexural uplift. In fact, localized flexural uplift at the scale of that observed in the Corinth Rift (~100 km) is suggested to report an isostatic elastic response of the whole crust that can only be achieved with high-angle crustal-scale planar faults (e.g., King and Ellis, 1990). Similarly, average fault dips (~50º; Nixon et al., 2016) and aspects ratios (displacement/length = 2,15; Nicol et al., 1996) result in fault tip depths that reach the crustal base (likely through more diffuse, ductile shear in the lower crust). In sum, the Corinth Rift active master fault transects with overall high-angle planar geometry at least until the brittle-ductile transition and well possibly the entire crust.

To conclude, while the older (>1 Ma) regional extension may be explained by basinwards fault migration with or without the mechanical aid of a shallow detachment (e.g., Goldsworthy and Jackson, 2001; Jolivet et al., 2010; Sorel, 2000), the evidence presented here for elastic flexure across the modern Corinth Rift indicates the growth of a new young (<1 Ma) steep rift-forming fault affecting the entire crust. Onset of such new fault may result from a sudden change in plate boundary conditions, possibly within the lithospheric-scale process zone associated with the southwestwards propagating tip of the North Anatolian Fault, as originally proposed by Armijo et al. (1996).

6. Conclusions

We analyse river catchments along strike of the Corinth Rift main shoulder to characterize a fluvial geomorphology that is consistent with a laterally-variable footwall elastic flexure along a new high-angle master fault. Elastic flexure of the footwall is asymmetrical along rift strike and reflects different master fault uplift rates and/or onset times; a higher uplift rate and/or older onset time in the central rift decays or becomes younger along strike, gently westwards and rapidly eastwards. An abrupt change in uplift rates in the master fault <1 Ma led to fast footwall flexure that forced river drainage reversals in the central rift and vigorous drainage reorganization still ongoing in the west. The abrupt growth of the modern master fault of the Corinth Rift and its associated flexure at the scale of the rift refutes models of continued rift growth, and suggests instead a genetic link with recent changes in plate boundary conditions possibly in relation with the North Anatolian Fault.

Acknowledgements

We are very thankful to two anonymous reviewers for their sharp comments that improved the quality of an early version of the paper. We are in debt with the editor, Rebecca Bendick. The research leading to these results has received funding from the People Programme (Marie Curie Actions) of the European Union's Seventh Framework Programme under the ITN project ALErT (Grant FP7-PEOPLE-2013-ITN number 607996) and by the ISIS program of CNES.

References

Armijo, R., Meyer, B., King, G.C.P., Rigo, A., Papanastassiou, D., 1996. Quaternary evolution of the Corinth Rift and its implications for the Late Cenozoic evolution of the Aegean. Geophys. J. Int. 126, 11–53.

Armijo, R., Tapponnier, P., Mercier, J.L., Han, T.-L., 1986. Quaternary extension in southern Tibet: Field observations and tectonic implications. J. Geophys. Res. 91, 13803–13872.

Avallone, A., Briole, P., Agatza-Balodimou, A.M., Billiris, H., Charade, O., Mitsakaki, C., Nercessian, A., Papazissi, K., Paradissis, D., Veis, G., 2004. Analysis of eleven years of deformation measured by GPS in the Corinth Rift Laboratory area. C. R. Geosci. 336, 301–311.

Bell, R.E., Mc Neill, L.C., Bull, J.M., Henstock, T.J., Collier, R.E.L., Leederz, M.R., 2009. Fault architecture, basin structure and evolution of the Gulf of Corinth Rift, central Greece. Basin Res. 21, 824–855.

Bell, R.E., McNeill, L.C., Henstock, T.J., Bull, J.M., 2011. Comparing extension on multiple time and depth scales in the Corinth Rift, Central Greece: Extension across the Corinth Rift. Geophys. J. Int. 186, 463–470.

Bell, R.E., Duclaux, G., Nixon, C.W., Gawthorpe, R.L., and McNeill, L.C., accepted, High-angle, not low-angle, normal faults dominate early rift extension in the Corinth Rift, central Greece: Geology (GSA), doi:10.1130/G39560.1

Bernard, P., Lyon-Caen, H., Briole, P., Deschamps, A., Boudin, F., Makropoulos, K., Papadimitriou, P., Lemeille, F., Patau, G., Billiris, H., Paradissis, D., Papazissi, K., Castarède, H., Charade, O., Nercessian, A., Avallone, A., Pacchiani, F., Zahradnik, J., Sacks, S., Linde, A., 2006. Seismicity, deformation and seismic hazard in the western rift of Corinth: New insights from the Corinth Rift Laboratory (CRL). Tectonophysics 426, 7–30.

Buck, W.R., 1993. Effect of lithospheric thickness on the formation of high- and low-angle normal faults. Geology 21, 933–936.

Buck, W.R., 1991. Modes of continental lithospheric extension. J. Geophys. Res. 96, 20161–20178.

Collier, R.E.L., Leeder, M.R., Rowe, P.J., Atkinson, T.C., 1992. Rates of tectonic uplift in the Corinth and Megara Basins, central Greece. Tectonics 11, 1159–1167.

Cowie, P.A., Attal, M., Tucker, G.E., Whittaker, A.C., Naylor, M., Ganas, A., and Roberts, G.P., 2006, Investigating the surface process response to fault interaction and linkage using a numerical modelling approach: Basin Research, v. 18, p. 231–266.

Cowie, P.A., and Scholz, C.H., 1992, Displacement-length scaling relationship for faults: data synthesis and discussion: Journal of Structural Geology, v. 14, p. 1149–1156.

Dawers, N.H., and Anders, M.H., 1995, Displacement-length scaling and fault linkage: Journal of Structural Geology, v. 17, p. 607–614.

de Gelder, G.I.N.O., Fernández-Blanco, D., Melnick, D., Duclaux, G., Bell, R.E., Jara-Muñoz, J., Armijo R., and Lacassin R., in rev "Fault flexure and lithosphere rheology set from climate cycles record in the Corinth Rift". Scientific Reports (ref nr: SREP-17-46566-T). Preprint, EarthArXiv (doi:10.17605/osf.io/4sh8e)

Densmore, A.L., Dawers, N.H., Gupta, S., Guidon, R., and Goldin, T., 2004, Footwall topographic development during continental extension: Journal of geophysical research, v. 109, p. F03001.

DiBiase, R.A., Whipple, K.X., 2011. The influence of erosion thresholds and runoff variability on the relationships among topography, climate, and erosion rate. J. Geophys. Res. 116, F04036.

Dufaure, J.-J., 1977. Néotectonique et morphogenèse dans une péninsule méditerranéenne: Le Péloponnèse. Revue de géographie physique et de géologie dynamique 19, 27–58.

Ford, M., Hemelsdaël, R., Mancini, M., Palyvos, N., 2016. Rift migration and lateral propagation: evolution of normal faults and sediment-routing systems of the western Corinth rift (Greece). Geological Society, London, Special Publications 439. doi:10.1144/SP439.15

Ford, M., Rohais, S., Williams, E.A., Bourlange, S., Jousselin, D., Backert, N., Malartre, F., 2012. Tectono-sedimentary evolution of the western Corinth rift (Central Greece). Basin Res. 25, 3–25.

Forsyth, D.W., 1992, Finite extension and low-angle normal faulting: Geology, v. 20, p. 27–30.

Gallen, S.F., Wegmann, K.W., 2017. River profile response to normal fault growth and linkage: An example from the Hellenic forearc of south-central Crete, Greece. Earth Surface Dynamics 5, 161–186.

Gawthorpe, R., Leeder, M., Kranis, H., Skourtsos, E., Andrews, J., Henstra, G., Mack, G., Muravchik, M., Turner, J., and Stamatakis, M., 2017, Tectono-sedimentary evolution of the Plio-Pleistocene Corinth rift, Greece: Basin Research, http://onlinelibrary.wiley.com/doi/10.1111/bre.12260/full.

Goldsworthy, M., Jackson, J., 2001. Migration of activity within normal fault systems: examples from the Quaternary of mainland Greece. J. Struct. Geol. 23, 489–506.

Jolivet, L., Labrousse, L., Agard, P., Lacombe, O., Bailly, V., Lecomte, E., Mouthereau, F., Mehl, C.,

2010. Rifting and shallow-dipping detachments, clues from the Corinth Rift and the Aegean. Tectonophysics 483, 287–304.
Karymbalis, E., Ferentinou, M., Giles, P.T., 2016a. Use of morphometric variables and self-organizing maps to identify clusters of alluvial fans and catchments in the north Peloponnese, Greece. Geological Society, London, Special Publications 440. doi:10.1144/SP440.7
King, G., Stein, R., and Rundle, J., 1988, The Growth of Geological Structures by Repeated Earthquakes 1. Conceptual Framework: Journal of Geophysical Research: Solid Earth, v. 93, p. 13307–13318.
King, G., Ellis, M., 1990. The origin of large local uplift in extensional regions. Nature 348, 689–693.
Kirby, E., Whipple, K., 2001. Quantifying differential rock-uplift rates via stream profile analysis. Geology 29, 415–418.
Kirby, E., Whipple, K.X., 2012. Expression of active tectonics in erosional landscapes. J. Struct. Geol. 44, 54–75.
McNeill, L.C., Collier, R.E.L., 2004. Uplift and slip rates of the eastern Eliki fault segment, Gulf of Corinth, Greece, inferred from Holocene and Pleistocene terraces. J. Geol. Soc. London 161, 81–92.
McNeill, L.C., Cotterill, C.J., Henstock, T.J., Bull, J.M., Stefatos, A., Collier, R.E.L., Papatheoderou, G., Ferentinos, G., Hicks, S.E., 2005. Active faulting within the offshore western Gulf of Corinth, Greece: Implications for models of continental rift deformation. Geology 33, 241–244.
Nicol, A., Watterson, J., Walsh, J.J., and Childs, C., 1996, The shapes, major axis orientations and displacement patterns of fault surfaces: Journal of Structural Geology, v. 18, p. 235–248.Nixon, C.W., McNeill, L.C., Bull, J.M., Bell, R.E., Gawthorpe, R.L., Henstock, T.J., Christodoulou, D., Ford, M., Taylor, B., Sakellariou, D., Ferentinos, G., Papatheodorou, G., Leeder, M.R., Collier, R.E.L.I., Goodliffe, A.M., Sachpazi, M., Kranis, H., 2016. Rapid spatiotemporal variations in rift structure during development of the Corinth Rift, central Greece. Tectonics 35, 2015TC004026.
Ori, G.G., 1989. Geologic history of the extensional basin of the Gulf of Corinth (?Miocene-Pleistocene), Greece. Geology 17, 918–921.
Perron, J.T., Royden, L., 2013. An integral approach to bedrock river profile analysis. Earth Surf. Processes Landforms.
Resor, P.G., and Pollard, D.D., 2012, Reverse drag revisited: Why footwall deformation may be the key to inferring listric fault geometry: Journal of Structural Geology, v. 41, p. 98–109.
Rigo, A., Lyon-Caen, H., Armijo, R., Deschamps, A., Hatzfeld, D., Makropoulos, K., Papadimitriou, P., Kassaras, I., 1996. A microseismic study in the western part of the Gulf of Corinth (Greece): Implications for large-scale normal faulting mechanisms. Geophys. J. Int. 126, 663–688.
Rohais, S., Eschard, R., Ford, M., Guillocheau, F., Moretti, I., 2007. Stratigraphic architecture of the Plio-Pleistocene infill of the Corinth Rift: Implications for its structural evolution. Tectonophysics 440, 5–28.
Rosenbloom, N.A., Anderson, R.S., 1994. Hillslope and channel evolution in a marine terraced landscape, Santa Cruz, California. J. Geophys. Res. 99, 14013–14029.
Sachpazi, M., Clément, C., Laigle, M., Hirn, A., Roussos, N., 2003. Rift structure, evolution, and earthquakes in the Gulf of Corinth, from reflection seismic images. Earth Planet. Sci. Lett. 216, 243–257.
Schwanghart, W., Scherler, D., 2014. Short Communication: TopoToolbox 2 – MATLAB-based software for topographic analysis and modeling in Earth surface sciences. doi:10.5194/esurf-2-1-2014
Seger, M., Alexander, J., 2009. Distribution of Plio-Pleistocene and Modern Coarse-Grained Deltas South of the Gulf of Corinth, Greece, in: Frostick, L.E. (Ed.), Tectonic Controls and Signatures in Sedimentary Successions (Special Publication 20 of the IAS). John Wiley & Sons, p. 37.
Snyder, N.P., Whipple, K.X., Tucker, G.E., Merritts, D.J., 2000. Landscape response to tectonic forcing: Digital elevation model analysis of stream profiles in the Mendocino triple junction region, northern California. Geol. Soc. Am. Bull. 112, 1250–1263.
Sorel, D., 2000. A Pleistocene and still-active detachment fault and the origin of the Corinth-Patras rift, Greece. Geology 28, 83–86.
Taylor, B., Weiss, J.R., Goodliffe, A.M., Sachpazi, M., Laigle, M., and Hirn, A., 2011, The structures,

stratigraphy and evolution of the Gulf of Corinth rift, Greece: Structures, stratigraphy and evolution of GoC: Geophysical Journal International, v. 185, p. 1189–1219.

Weissel, J.K., and Karner, G.D., 1989, Flexural uplift of rift flanks due to mechanical unloading of the lithosphere during extension: Journal of geophysical research, v. 94, p. 13919–13950.

Whipple, K.X., Tucker, G.E., 1999. Dynamics of the stream-power river incision model: Implications for height limits of mountain ranges, landscape response timescales, and research needs. J. Geophys. Res. [Solid Earth] 104, 17661–17674.

Willett, S.D., McCoy, S.W., Perron, J.T., Goren, L., Chen, C.-Y., 2014. Dynamic reorganization of river basins. Science 343, 1248765.

Whittaker, A.C., Attal, M., Cowie, P.A., Tucker, G.E., and Roberts, G., 2008, Decoding temporal and spatial patterns of fault uplift using transient river long profiles: Geomorphology , v. 100, p. 506–526.

Wobus, C., Whipple, K.X., Kirby, E., Snyder, N., Johnson, J., Spyropolou, K., Crosby, B., Sheehan, D., 2006. Tectonics from topography: Procedures, promise, and pitfalls. Geological Society of America Special Papers 398, 55–74.

Supplementary material

A. River profile analysis

Researchers have demonstrated that there is a functional relationship between rock uplift rate or erosion rate and river channel steepness normalized upstream by contributing drainage area, which suggests that river channel steepness can be used as a proxy for relative rate of uplift or erosion (DiBiase et al., 2010; Gallen and Wegmann, 2017; Ouimet et al., 2009; Snyder et al., 2000). These empirical studies are supported by quasi-physical models of river incision that imply that bedrock river incision is related to upstream drainage area, a proxy for discharge, and local channel slope (Howard, 1994; Tucker and Whipple, 2002; Whipple and Tucker, 1999). The most general of these models is the detachment-limited stream power incision model, which, when combined with mass-conservation, describes the change in river bed elevation over time as follows,

$$\frac{dz}{dt} = U - E = U - KA^m S^n \quad (1)$$

where *dz/dt* is the change in elevation of the channel bed with time, U is rock uplift rate relative to a fixed base level, E is river erosion, A is the upstream drainage area, S is local channel slope, K is a dimensional coefficient that incorporates variables dependent on incision process, substrate, climate and hydrology of erosion (e.g., Whipple, 2004), and m and n are positive constants that depend on basin hydrology, channel geometry, and erosion processes (Howard, 1994; Whipple, 2004; Whipple and Tucker, 1999). Assuming steady-state conditions where rock uplift rate and erosion rate are equal, local channel slope can be cast as a function as,

$$S = (U/K)^{1/n} A^{-(m/n)} \quad (2)$$

Equation 2 has the same form as Flint's (1974) law, which describes the equilibrium geometry of a longitudinal river profile as a power law function of upstream contributing drainage area through the

channel parameters of the steepness index and concavity index. The steepness index is proportional to the ratio of rock uplift to substrate erodibility and the concavity index is equal to the ratio of m to n (Kirby and Whipple, 2001; Snyder et al., 2000).

The river channel concavity, defined as or m/n, is theoretically independent of rock uplift rate or erosion rate but will strongly impact the steepness index of the river. In an effort to remove the influence of channel concavity on the steepness index many researchers use a fixed reference concavity index, defined as θ (m/n), to derive a normalized steepness index, k_{sn}. From theory, the concavity index (θ) should vary between ~0.3 to 0.7, and many empirical studies find a value of ~0.45 for most river profiles near equilibrium or graded conditions (Kirby and Whipple, 2012; Snyder et al., 2000; Wobus et al., 2006). Thus, most researchers use a reference concavity of 0.45, as is used in this study, to calculate the normalized steepness index and assess relative patterns of rock uplift in space and time.

Traditionally, k_{sn} is calculated by a linear regression of $log\, S$ and $log\, A$ (Kirby and Whipple, 2012); however, Perron and Royden (2013) recognized that this approach introduces unwanted noise in the data and they propose the integral or χ method of river profile analysis instead. The χ-analysis relies on a transformation of the horizontal coordinate for a river profile, from distance to χ, where χ is an integral quantity with units of length. Separating variables in Eq (2), assuming U and K are spatially invariant, and integrating yields:

$$z(x) = z(x_b) + \left(\frac{U}{K}\right)^{\frac{1}{n}} \int_{x_b}^{x} \frac{dx}{A(x)^{m/n}} \quad (3)$$

Where z is elevation and x_b is base level. The trailing term on the right-hand side of the equation is unitless. Therefore, a reference drainage area A_o is introduced such that:

$$z(x) = z(x_b) + \left(\frac{U}{KA_o^m}\right)^{\frac{1}{n}} \chi \quad (4)$$

Where:

$$\chi = \int_{x_b}^{x} \left(\frac{A_o}{A(x)}\right)^{m/n} \quad (5)$$

Equation 7 is convenient because it has the form of a line where z is the dependent variable, χ is the independent variable, $z(x_b)$ is the y-intercept and $\left(\frac{U}{KA_o^m}\right)^{\frac{1}{n}}$ is the slope. Plots of χ and z are referred to as χ-plots. It is important to recognize that when A_o is assumed to be 1 the slope in a χ-plot is the same as k_{sn}, thus it is best practice to always use an A_o equal to 1 to standardize χ-plots (e.g., Gallen and Wegmann, 2017). We emphasize that, while the above derivation assumes that U and K are spatially uniform, we are only using χ-plots to assess geometric changes in the river profile geometry. Variability observed in the river profile geometry of χ-plots may be attributed to spatial and/or temporal changes in rock uplift rate and/or erodibility.

First order clues on the evolution of normal fault systems can be deduced from local convexities (knickpoints zones) in the longitudinal profiles of footwall rivers. For example, a change in rock uplift rate will lead to the upstream migration of a knickpoint as a kinematic-wave, and the river channel will steepen in the wave of the knickpoint (Rosenbloom and Anderson, 1994). The knickpoint acts hence as a mobile boundary between a former portion of the stream unaware of a change in uplift rate and an adjusted or adjusting downstream reach (e.g., Snyder et al., 2000; Whipple and Tucker, 1999).

We generate χ-plots and maps of k_{sn} from χ-elevation data. χ is calculated by intergating drainage area with respect to local base level, using an A_o of 1 and m/n of 0.45. The river network is defined as areas that are draining ≥ 10^6 m^2. Maps of k_{sn} were generated by performing a linear regression through χ and channel elevation data along 500 m channel segments.

We used the available ASTER GDEM V2 and ALOS AW3D30 DSM (ASTER; ALOS) at 30 m horizontal resolution, and acquired SPOT5 DEM at 20 m horizontal (post-spacing) resolution. We filled the ALOS DSM voids and gaps with ASTER GDEM, for an area inclusive of the whole Peloponnese and both margins of the Gulf of Corinth. We clipped the merged DEM for latitudes northern than Nafplion

and upsampled it with a SPOT5 DEM that covers the majority of the southern shoulder of the Gulf of Corinth, the Perachora Peninsula and the Kaparelli area (see bottom-left inset in Fig. 1). We further clipped the composite DEM with the area defined by the drainages of Peloponnesian river discharging into the gulf and the three inverted endorheic basins of Feneos, Stymfalia and Skotini. This area was manually delineated to avoid inaccuracies of automatic methods. To protray river network morphology and the longitudinal profiles of the aforementioned endorheic catchments, which flow do not reach the regional base level, we performed specific corrections. We set an artificial outlet by creating a sink at the lowest point of the longest stream, and clipped the DEM in the two drainage areas draining towards it. We performed stream flow direction and other suitable procedures as for the rest of the rivers. We oriented the outcome of the longitudinal river profiles according to their geography, i.e. one flowing northwards and one southwards. The resulting longitudinal profile was oriented to match the flow direction in the longitudinal profiles of exorheic rivers.

B. River profile response to flexural uplift

To provide a conceptual framework from which to interpret river profile morphology in the Gulf of Corinth we use a simple 1-D finite difference forward in time numerical model to simulate river profile response flexural uplift of a hypothetical footwall. River incision is cast as in equation 1 and flexural uplift (Turcotte and Schubert 2002) is simulated as,

$$U(x) = U_{max}\cos\left({}^{x}/_{\alpha}\right)e^{-{}^{x}/_{\alpha}} \quad (6)$$

Where U_{max} is the maximum uplift, x is distance perpendicular to fault strike and α is the flexural parameter defined as,

$$\alpha = \left(\frac{4D}{\rho_f g}\right)^{\frac{1}{4}} \quad (7)$$

Where ρ_f is the density of the fill (assumed to be 2700 kg·m^{-3}), g is gravity (9.81 m·s^{-2}), and D is the

flexural rigidity,

$$D = \frac{ET_e^3}{12(1-\nu^2)} \quad (8)$$

Where E is Youngs Modulus (65 Gpa), T_e is the effective elastic thickness (2 km), and ν is Poisson's ratio (0.25).

The river channel drainage area is approximated using the inverse of Hack's law with a scaling constant of 6.67 and an exponent of 1.67. The drainage area and slope exponents in the stream power model are set to 0.5 and 1.0, respectively. The model is run for 7.5 Ma and the transient profile (gray lines) are plotted every 937.5 kyr. In the model we assume that bedrock erodibility for river incision is constant at 10^{-6} yr^{-1} and an initially spatially uniform rock uplift rate of 0.2 $mm \cdot yr^{-1}$. The uplift rate is quadrupled to 0.8 $mm \cdot yr^{-1}$ at the mouth of the river and decays to a minimum value of 0.2 $mm \cdot yr^{-1}$ following Eq (6) in 25 km, following the flexural uplift decay estimated by previous workers (Armijo et al, 1996; de Gelder et al, in rev.). The model is designed for conceptual purposed only and is not intended to be specifically representative of the Gulf of Corinth.

C. Supplementary Material C to R – River catchments maps and profiles

Caption valid for supplementary figures from C to R.

Main features of the studied river networks. Up left shows the location of the river network in the context of the southern shoulder of the Corinth Rift. Up right is a map view of the river drainage and network over the geology. In the bottom line, from left to right, are the longitudinal river profile, the χ-profile, and the slope-area log-log plot.

S. River profile changes in response to other footwall uplift scenarios

We have run two extra different models (based on similar theoretical considerations -suppl. material A and B-) to simulate other potential scenarios of footwall uplift.

Model S-1 reproduces several linear signals of uplift rate decay along the length of a river profile, as expected from proposed block-tilt models of the Corinth Rift (see Ford et al., 2016, Figs. 3 and 4 for the west; and Gawthorpe et al., 2017, Fig. 2-b, for the central rift). Although lengths represented for such blocks in the cross sections for the Corinth Rift are around to 5 km in length, we used tilted blocks of 10 km in length, since smaller blocks produced unrealistic river profiles. The outcome of this model is still very unrealistic and does not resemble any of the rivers in the Corinth Rift.

Model S-2 reproduces a linear decay in uplift rate away from the main fault equivalent to the full length of the river profile. This model implies that a linear uplift decay will equally serve to explain the observed morphology than a flexural decay if the decay occurs along the full length of the river. The natural equivalent of this model in the Corinth Rift would be produced by a tilted block of 50 km in length. This is, to our knowledge, not shown by any study in the Corinth Rift.

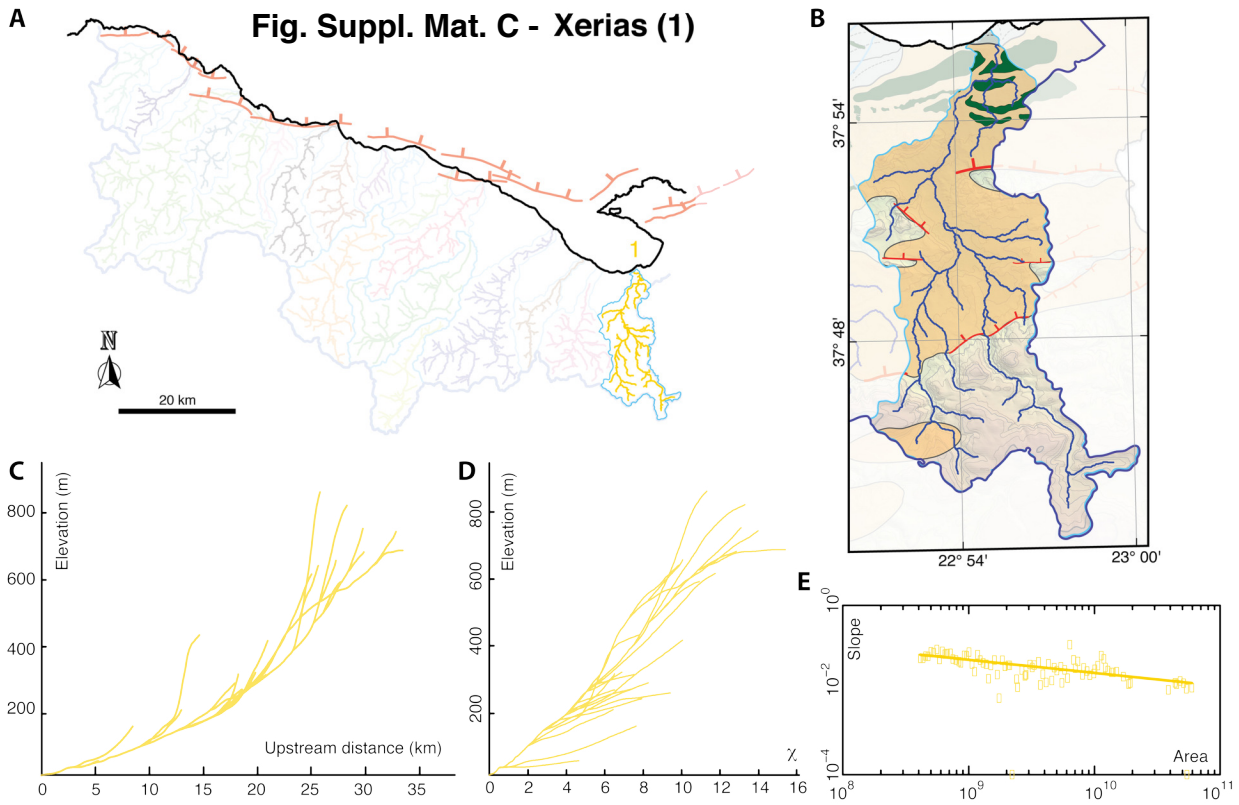
A
Fig. Suppl. Mat. C - Xerias (1)
1
N
20 km
B
37° 54'
37° 48'
22° 54'
23° 00'
C
Elevation (m)
800
600
400
200
Upstream distance (km)
0 5 10 15 20 25 30 35
D
Elevation (m)
800
600
400
200
χ
0 2 4 6 8 10 12 14 16
E
Slope
10^{0}
10^{-2}
10^{-4}
Area
10^{8} 10^{9} 10^{10} 10^{11}

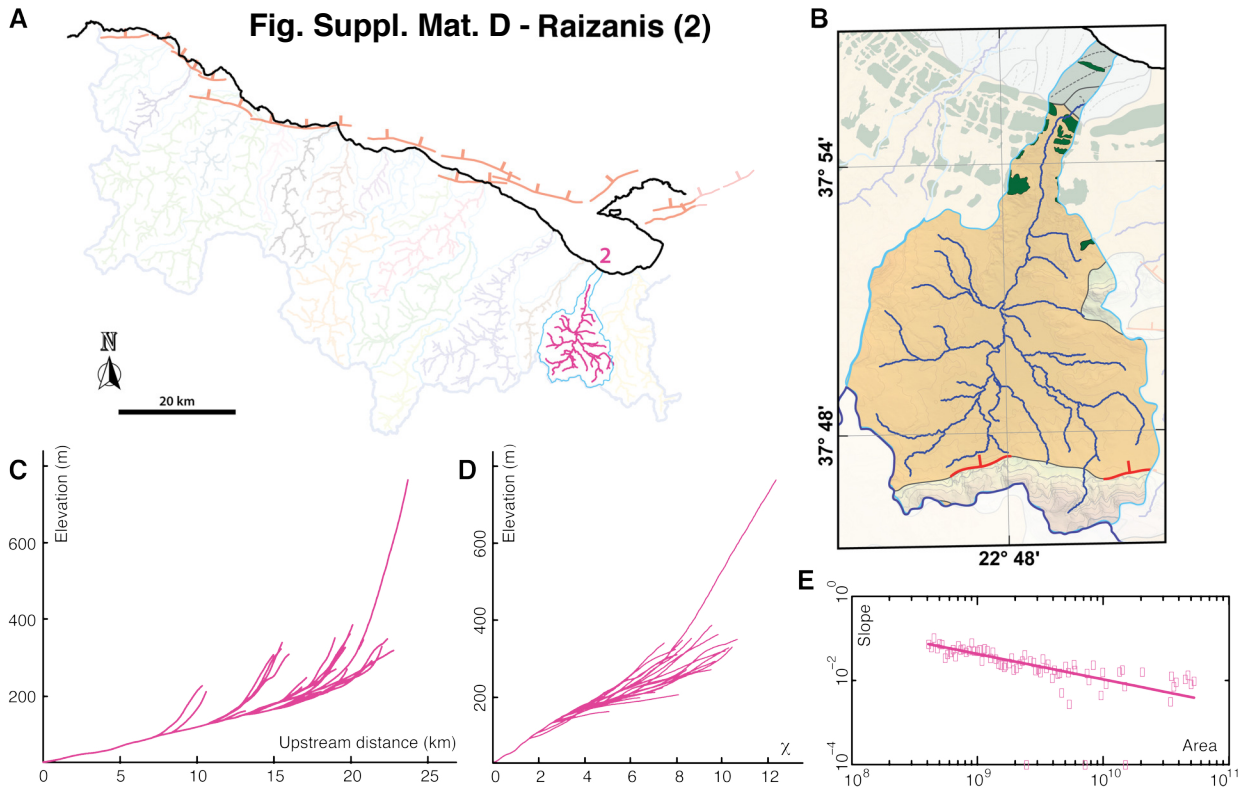
A
Fig. Suppl. Mat. D - Raizanis (2)
2
N
20 km
B
37° 54'
37° 48'
22° 48'
C
Elevation (m)
600
400
200
Upstream distance (km)
0 5 10 15 20 25
D
Elevation (m)
600
400
200
χ
0 2 4 6 8 10 12
E
Slope
10^{0}
10^{-2}
10^{-4}
Area
10^{8} 10^{9} 10^{10} 10^{11}

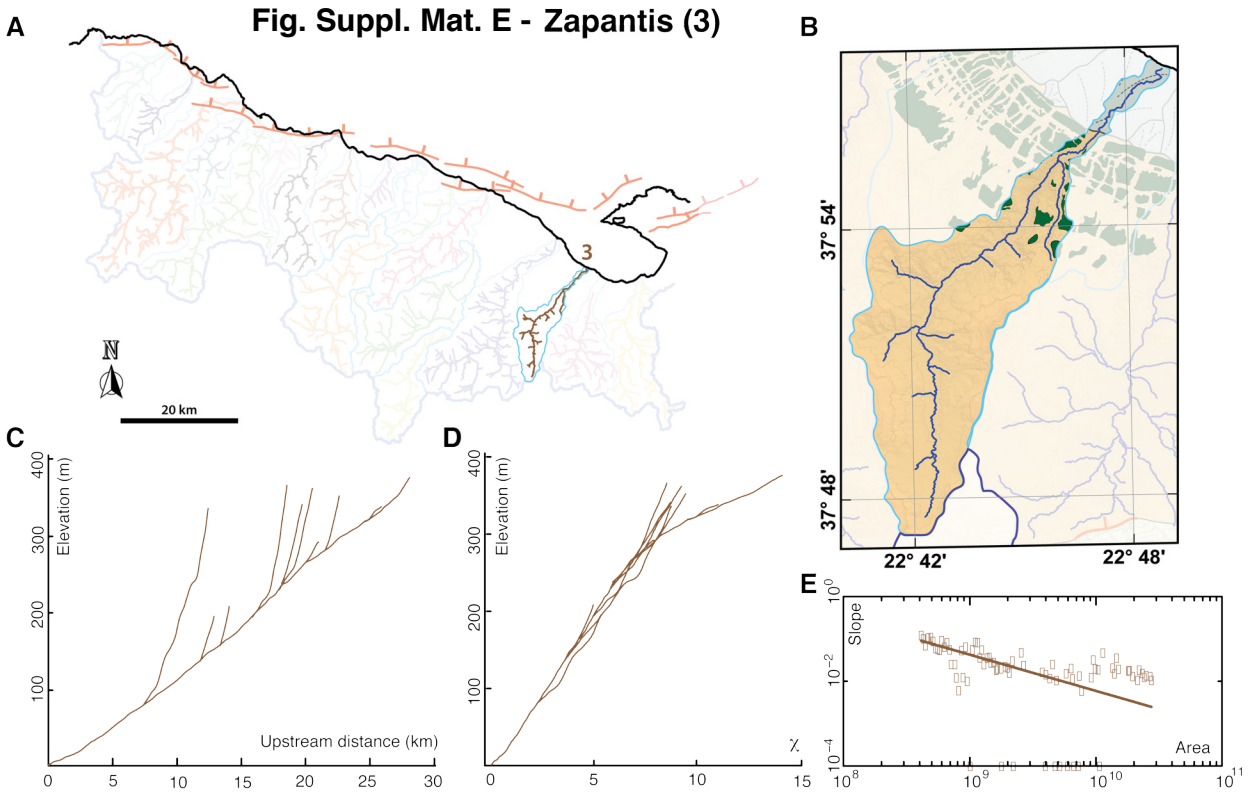
Fig. Suppl. Mat. E - Zapantis (3)
A
B
C
D
E
3
N
20 km
Elevation (m)
Upstream distance (km)
χ
Slope
Area
37° 54'
37° 48'
22° 42'
22° 48'

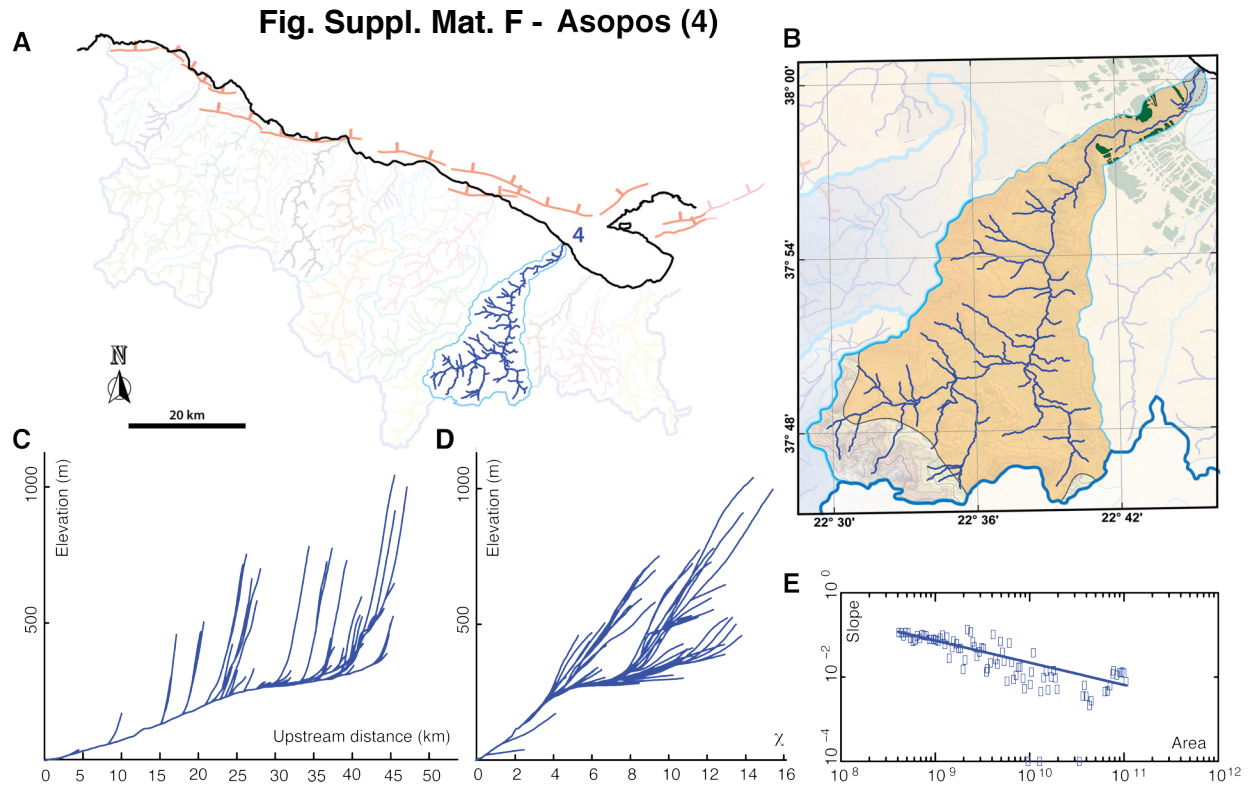
Fig. Suppl. Mat. F - Asopos (4)
A
B
C
D
E
4
N
20 km
Elevation (m)
Upstream distance (km)
χ
Slope
Area
38° 00'
37° 54'
37° 48'
22° 30'
22° 36'
22° 42'

Fig. Suppl. Mat. G - Trikalitikos (5)

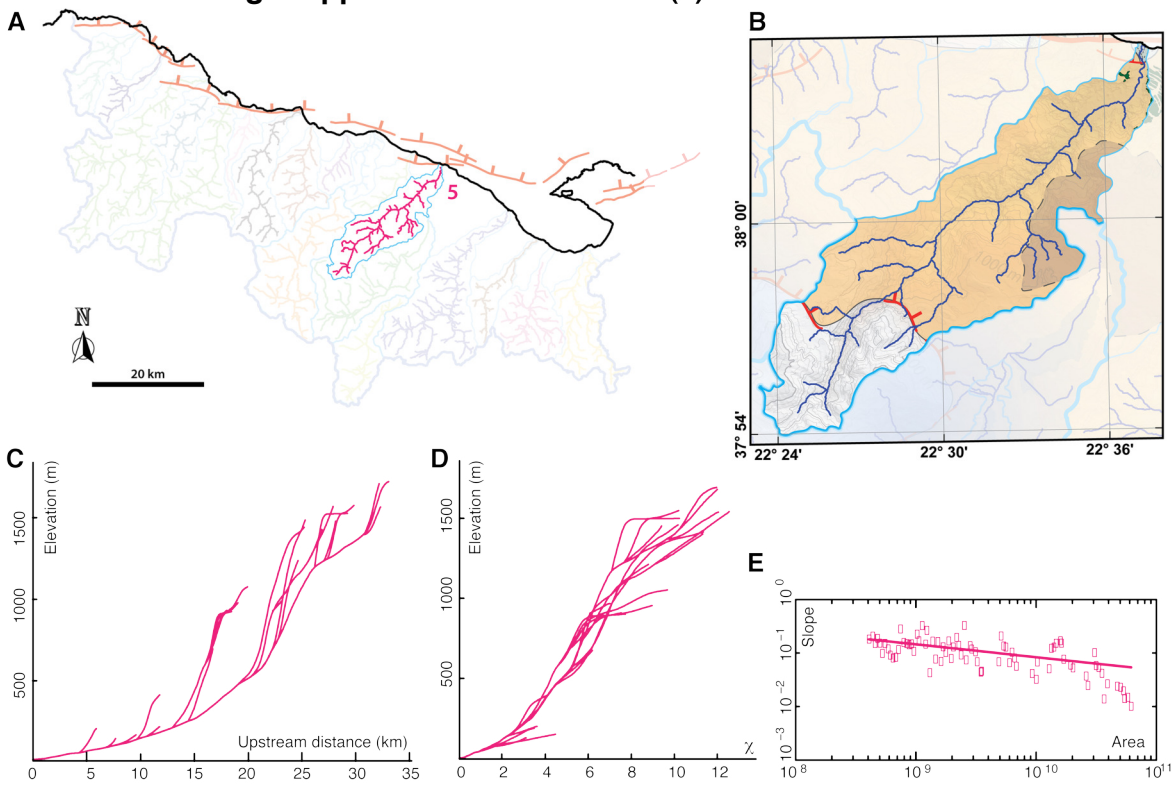

Fig. Suppl. Mat. H - Fonissa (6)

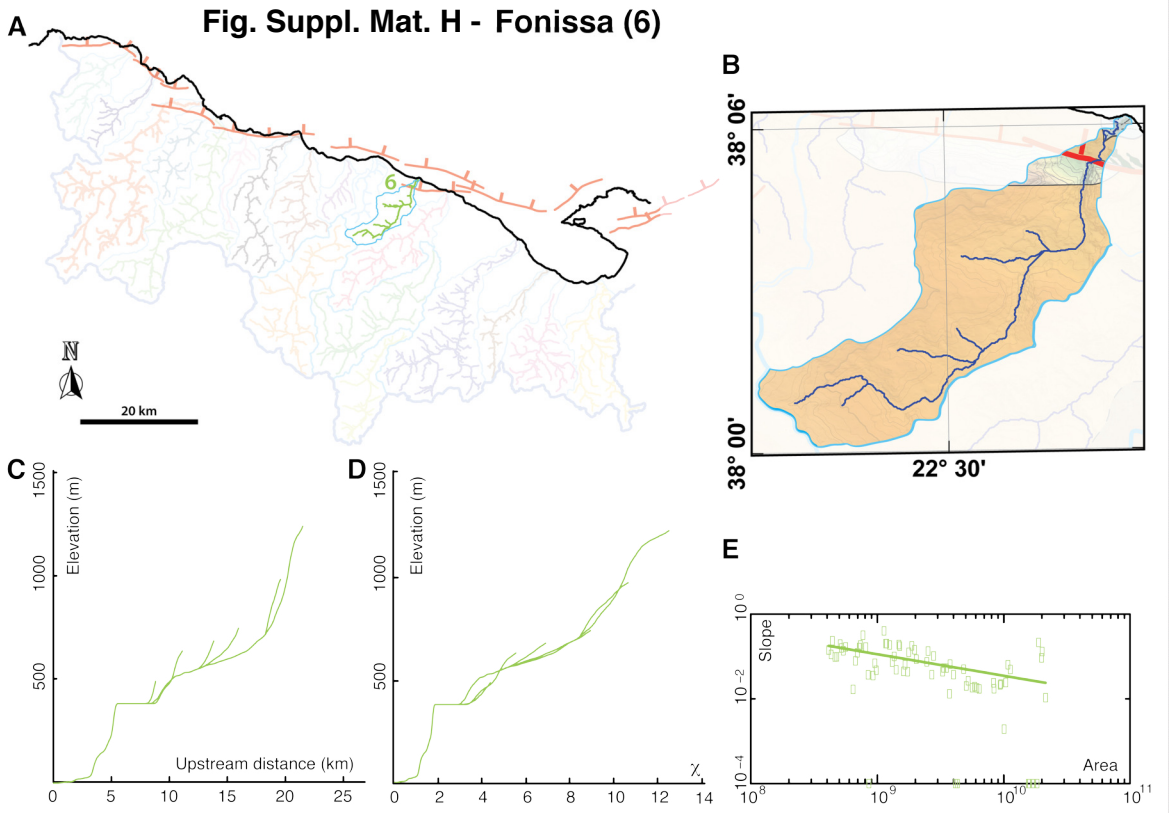

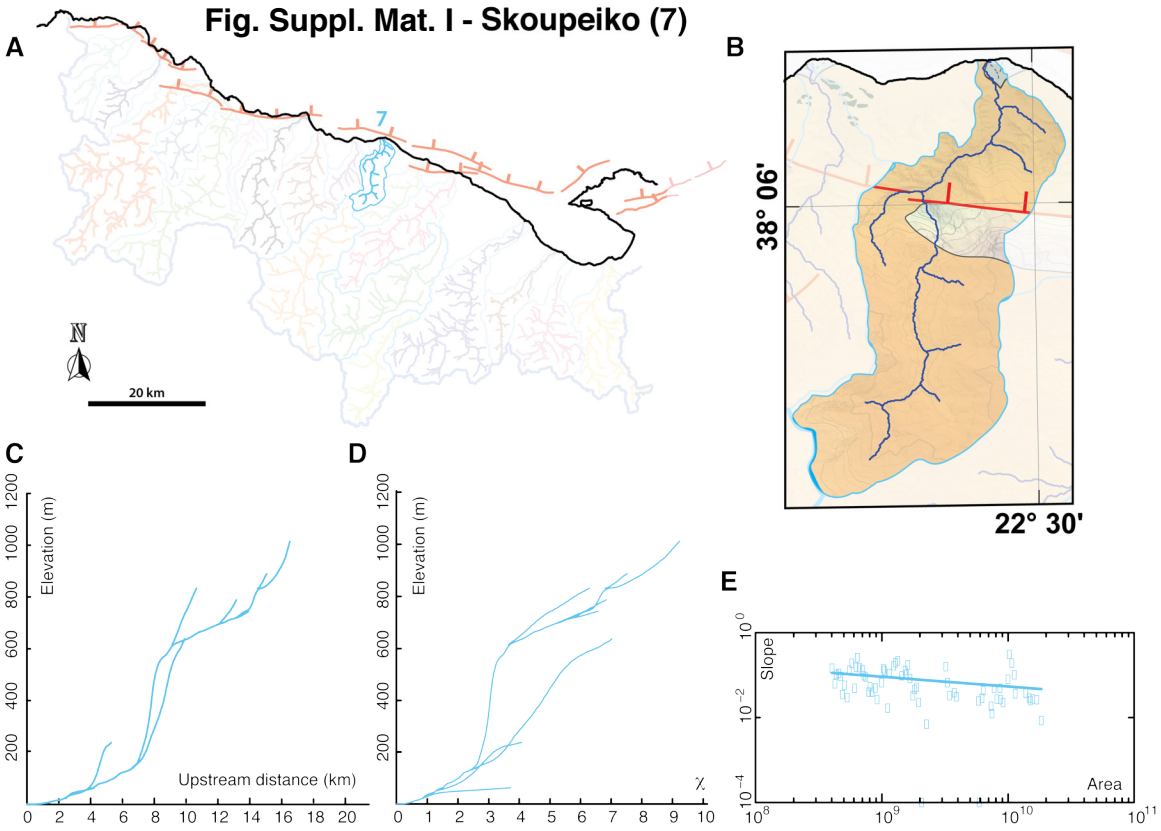
Fig. Suppl. Mat. I - Skoupeiko (7)
A
7
N
20 km
B
38° 06'
22° 30'
C
Elevation (m)
Upstream distance (km)
D
Elevation (m)
χ
E
Slope
Area

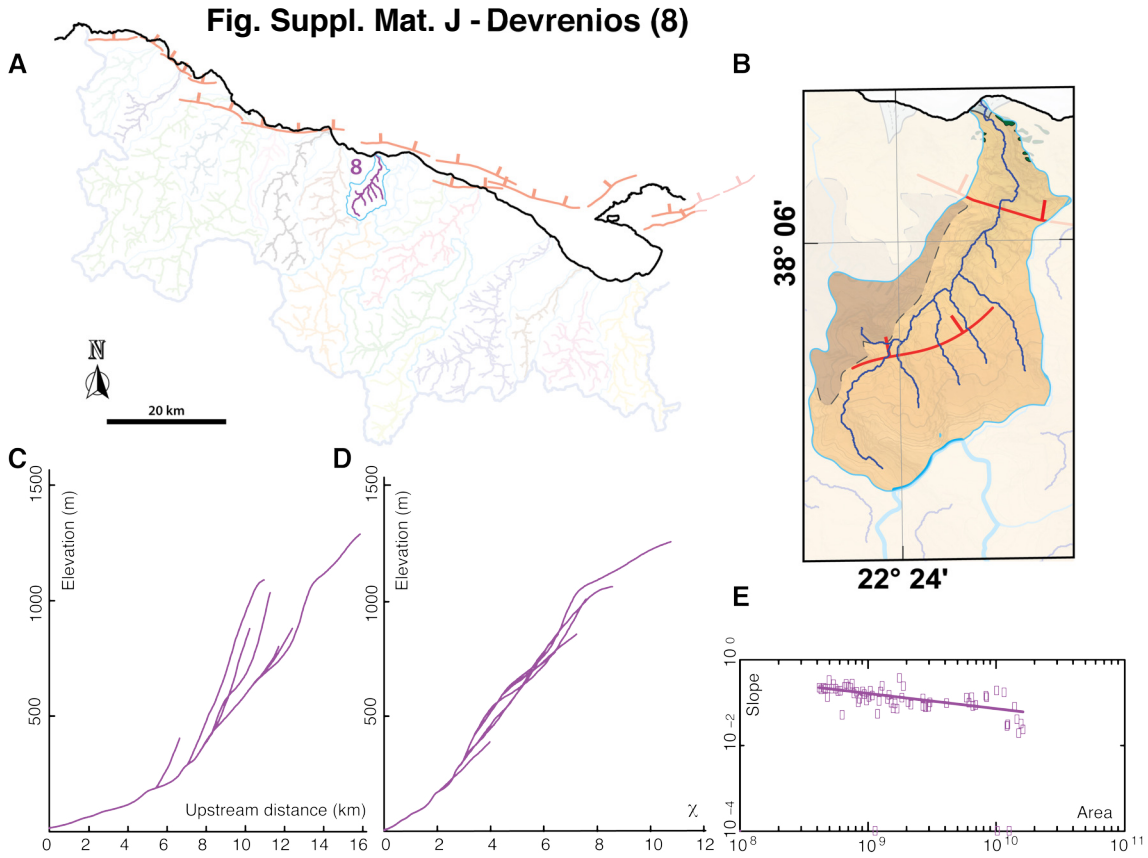
Fig. Suppl. Mat. J - Devrenios (8)
A
8
N
20 km
B
38° 06'
22° 24'
C
Elevation (m)
Upstream distance (km)
D
Elevation (m)
χ
E
Slope
Area

Fig. Suppl. Mat. K - Krios (9)

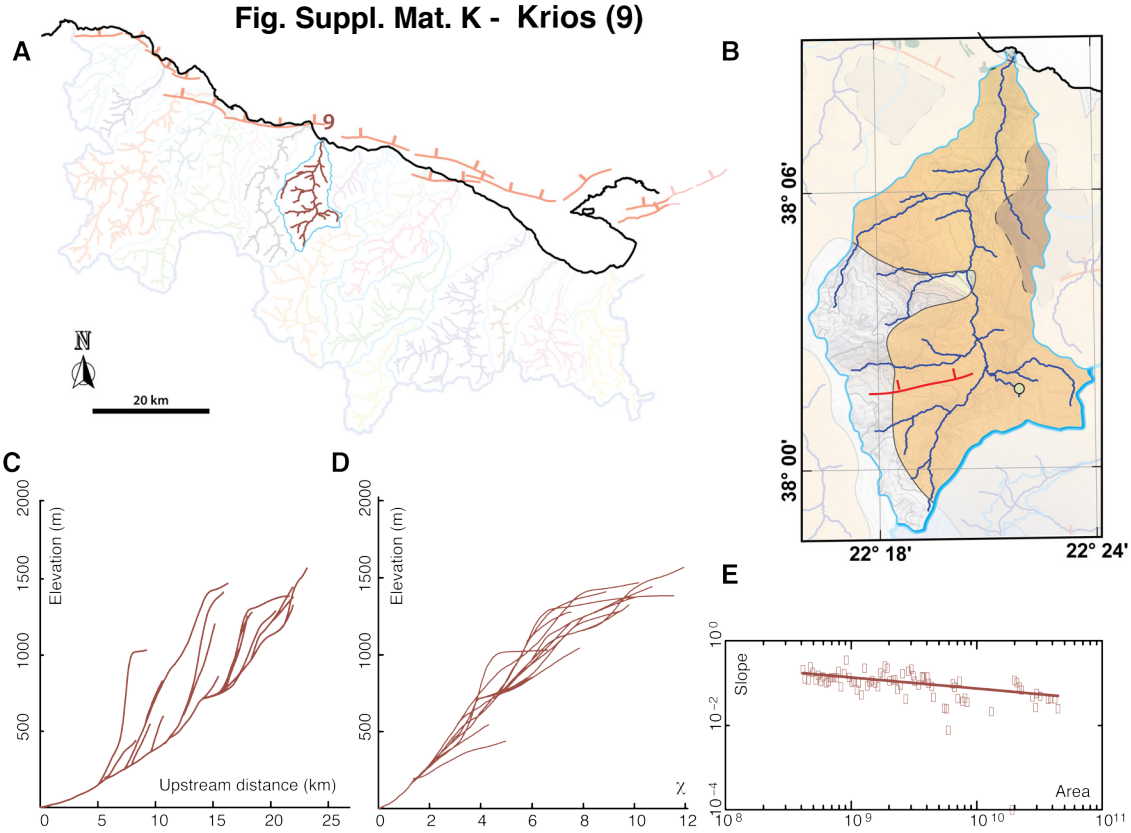

Fig. Suppl. Mat. L - Krathis (10)

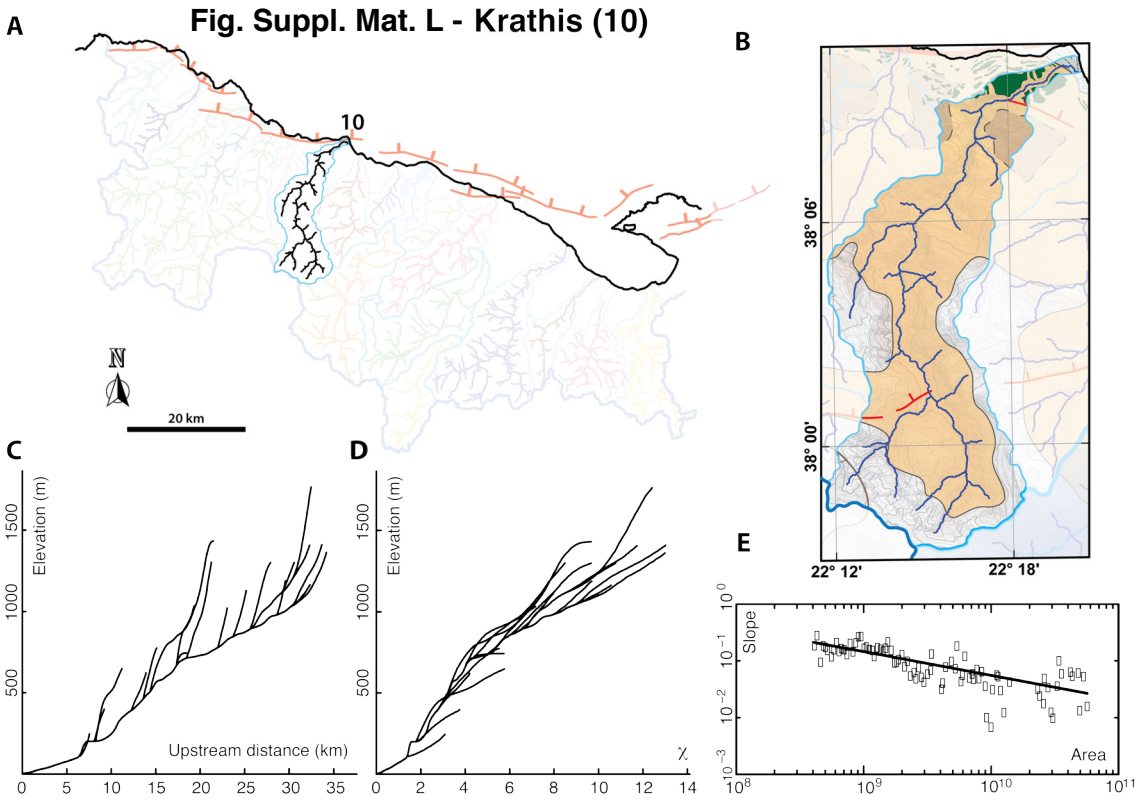

Fig. Suppl. Mat. M - Ladopotamos (11)

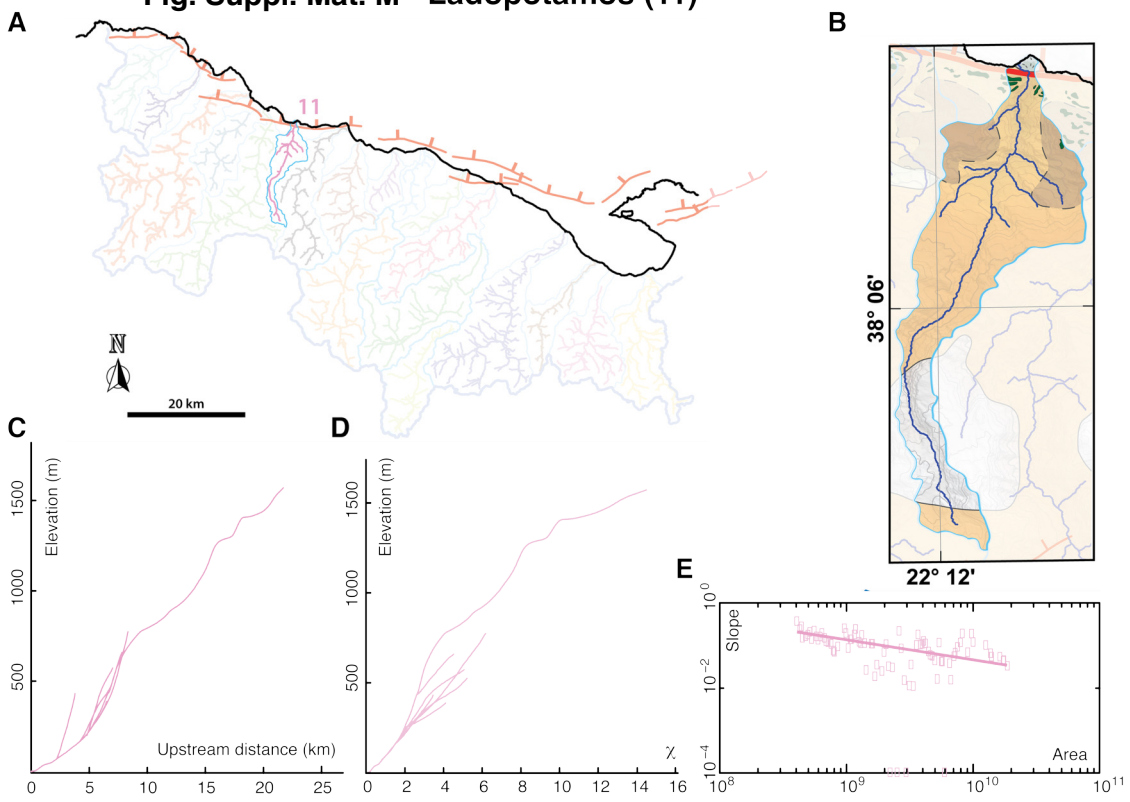

Fig. Suppl. Mat. N - Vouraikos (12)

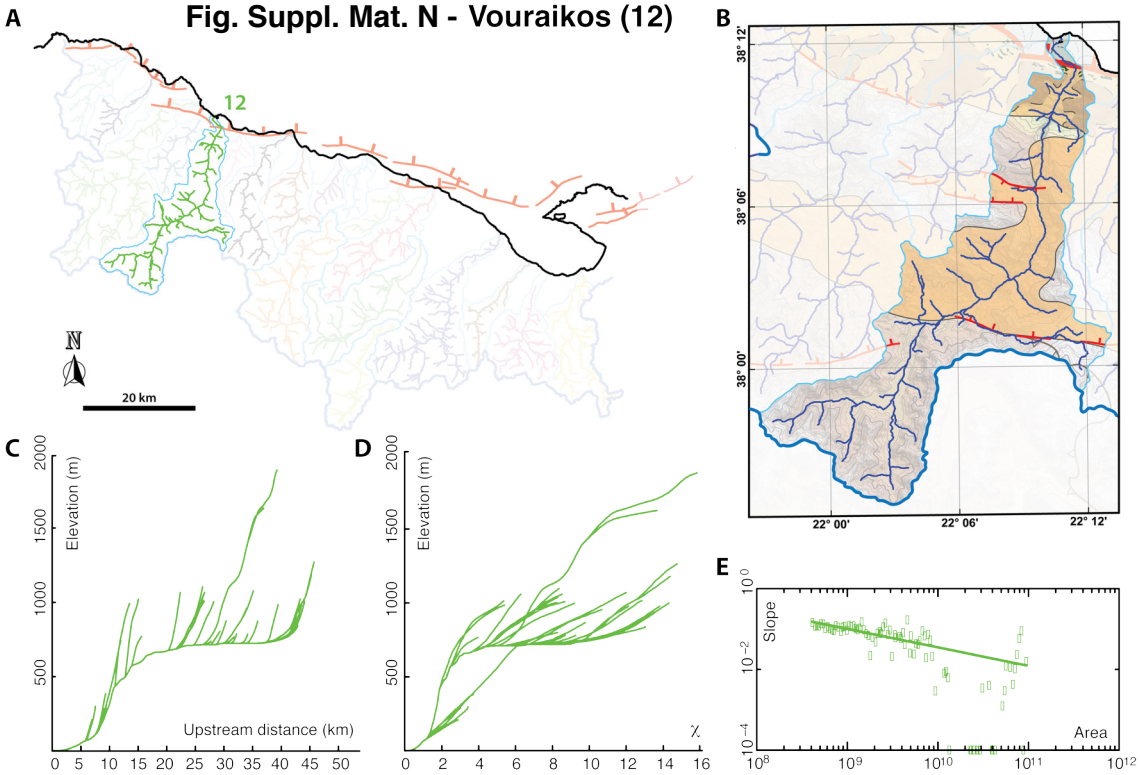

Fig. Suppl. Mat. O - Kerinitis (13)

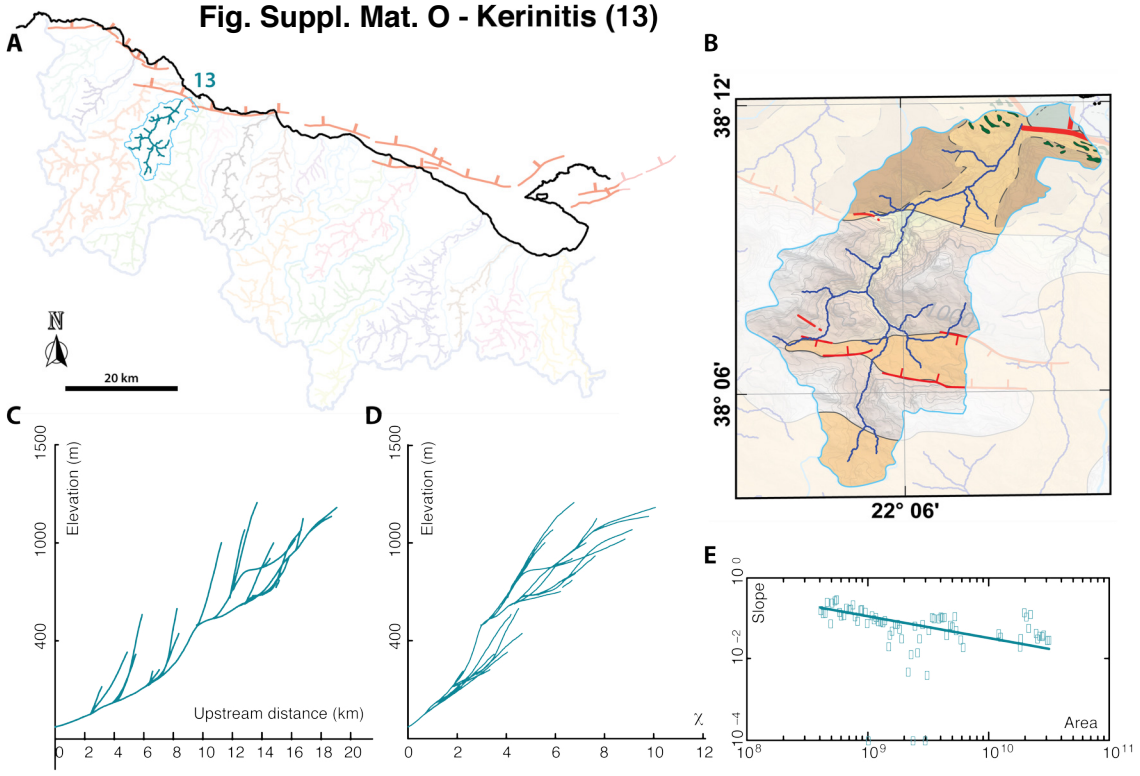

Fig. Suppl. Mat. P - Selinous (14)

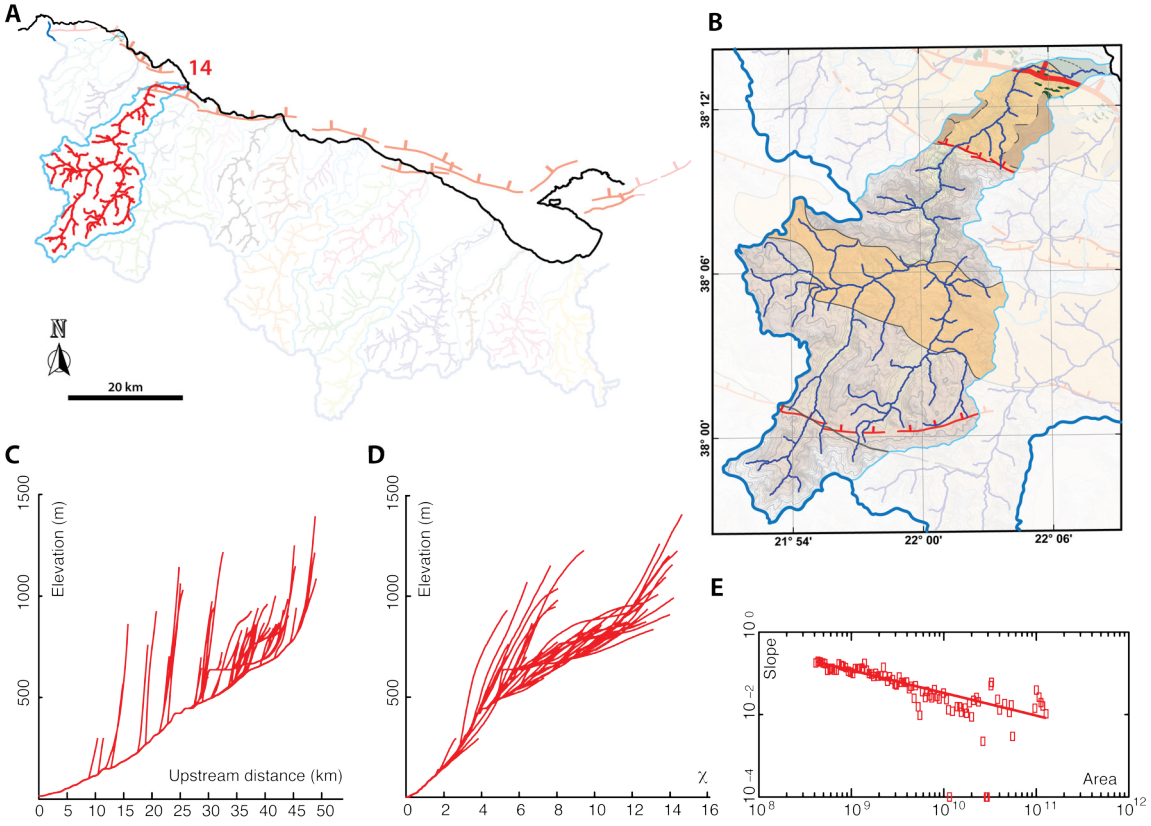

Fig. Suppl. Mat. Q - Meganitis (15)

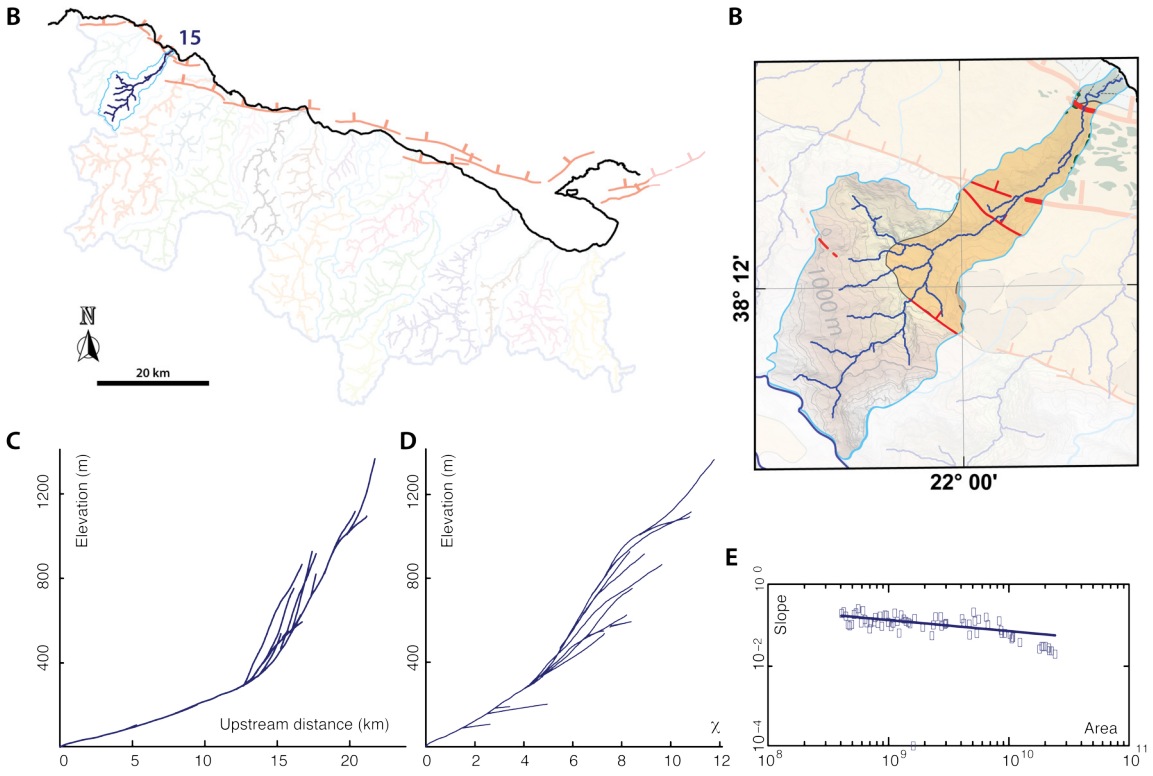

Fig. Suppl. Mat. R - Finikas (16)

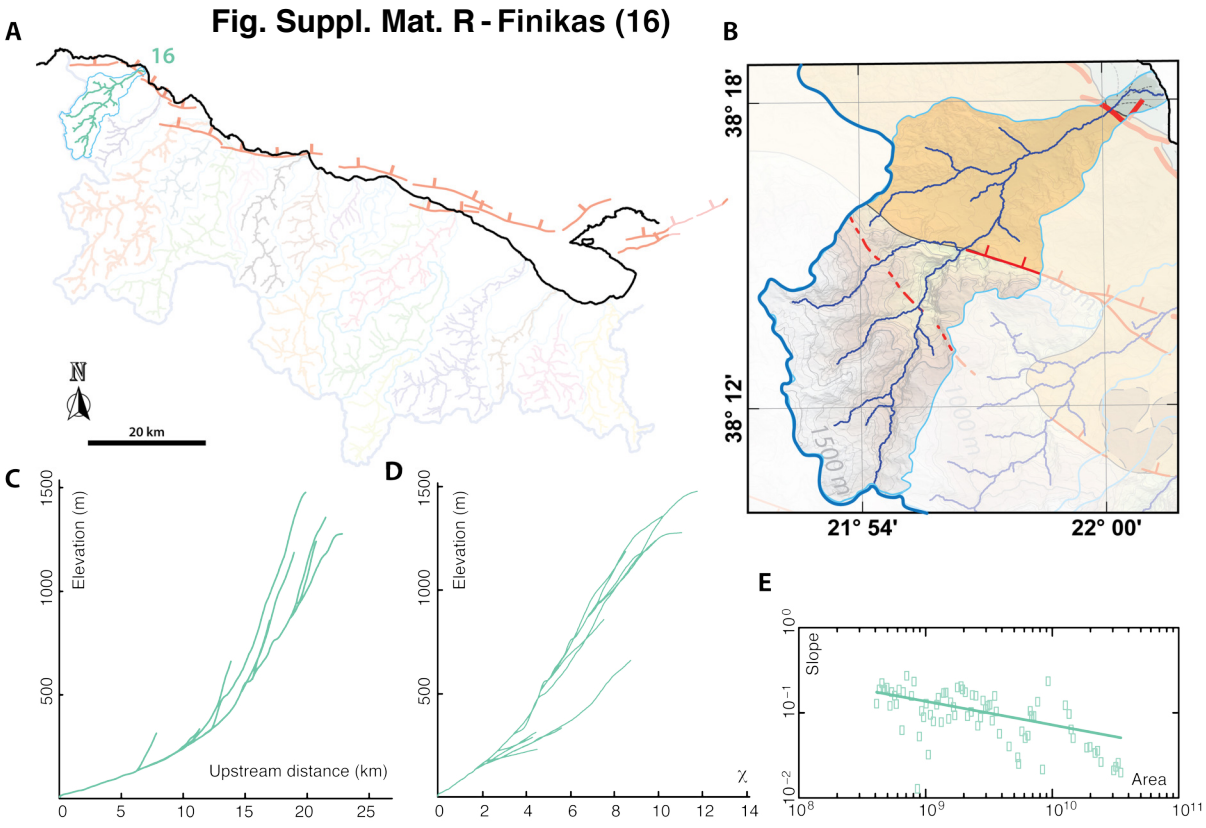

Figure Supplementary Material S

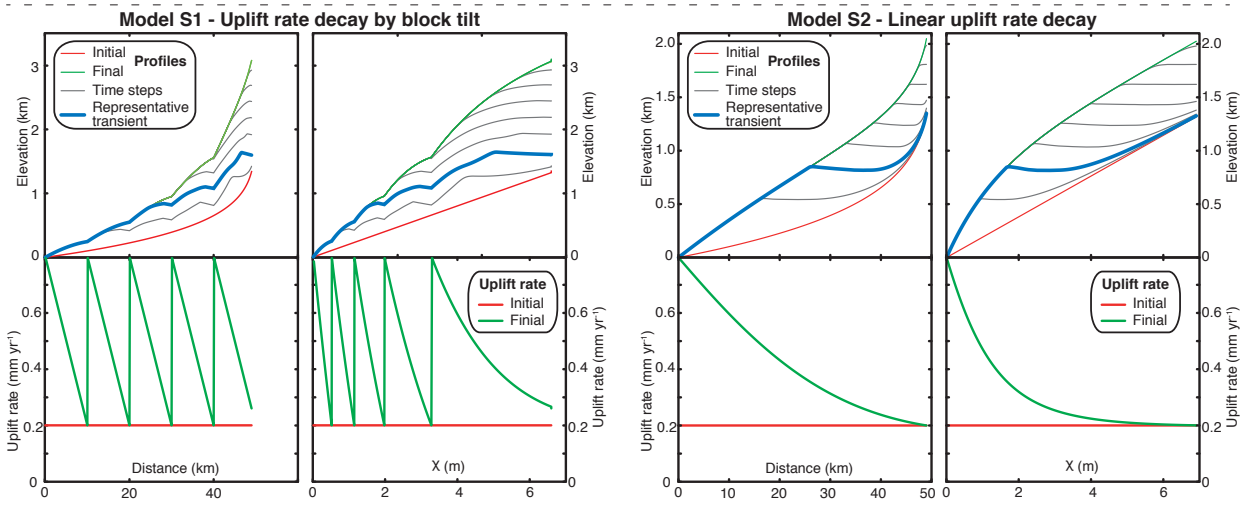

References (Supplementary material)

DiBiase, R.A., Whipple, K.X., Heimsath, A.M., Ouimet, W.B., 2010. Landscape form and millennial erosion rates in the San Gabriel Mountains, CA. Earth Planet. Sci. Lett. 289, 134–144.

Flint, J.J., 1974. Stream gradient as a function of order, magnitude, and discharge. Water Resour. Res. 10, 969–973.

Gallen, S.F., Wegmann, K.W., 2017. River profile response to normal fault growth and linkage: An example from the Hellenic forearc of south-central Crete, Greece. Earth Surface Dynamics 5, 161.

Howard, A.D., 1994. A detachment-limited model of drainage basin evolution. Water Resour. Res. 30, 2261–2285.

Kirby, E., Whipple, K., 2001. Quantifying differential rock-uplift rates via stream profile analysis. Geology 29, 415–418.

Kirby, E., Whipple, K.X., 2012. Expression of active tectonics in erosional landscapes. J. Struct. Geol. 44, 54–75.

Ouimet, W.B., Whipple, K.X., Granger, D.E., 2009. Beyond threshold hillslopes: Channel adjustment to base-level fall in tectonically active mountain ranges. Geology 37, 579–582.

Perron, J.T., Royden, L., 2013. An integral approach to bedrock river profile analysis. Earth Surface Processes and Landforms 38, 570–576.

Rosenbloom, N.A., Anderson, R.S., 1994. Hillslope and channel evolution in a marine terraced landscape, Santa Cruz, California. J. Geophys. Res. 99, 14013–14029.

Snyder, N.P., Whipple, K.X., Tucker, G.E., Merritts, D.J., 2000. Landscape response to tectonic forcing: Digital elevation model analysis of stream profiles in the Mendocino triple junction region, northern California. Geol. Soc. Am. Bull. 112, 1250–1263.

Tucker, G.E., Whipple, K.X., 2002. Topographic outcomes predicted by stream erosion models: Sensitivity analysis and intermodel comparison. J. Geophys. Res. 107, 2179.

Turcotte, D.L., Schubert, G., 2002. Elasticity and Flexure, in: Turcotte, D.L., Schubert, G. (Eds.), Geodynamics. Cambridge University Press, Cambridge, pp. 105–131.

Whipple, K.X., 2004. Bedrock rivers and the geomorphology of active orogens. Annu. Rev. Earth Planet. Sci. 32, 151–185.

Whipple, K.X., Tucker, G.E., 1999. Dynamics of the stream-power river incision model: Implications for height limits of mountain ranges, landscape response timescales, and research needs. J. Geophys. Res. [Solid Earth] 104, 17661–17674.

Wobus, C., Whipple, K.X., Kirby, E., Snyder, N., Johnson, J., Spyropolou, K., Crosby, B., Sheehan, D., 2006. Tectonics from topography: Procedures, promise, and pitfalls. Geological Society of America Special Papers 398, 55–74.